Spatiotemporal transcriptome of the human brain

Hyo Jung Kang[1*], Yuka Imamura Kawasawa[1*], Feng Cheng[1*], Ying Zhu[1*], Xuming Xu[1], Mingfeng Li[1], André M. M. Sousa[1,2], Mihovil Pletikos[1,3], Kyle A. Meyer[1], Tobias Guennel[4], Goran Sedmak[1,3], Yurae Shin[1], Matthew B. Johnson[1], Željka Krsnik[1], Sofia Fertuzinhos[1], Sheila Umlauf[5], Alexander Vortmeyer[6], Daniel R. Weinberger[7], Shrikant Mane[5], Thomas M. Hyde[7,8], Anita Huttner[6], Mark Reimers[4], Joel E. Kleinman[7], Nenad Šestan[1]

[1]Department of Neurobiology and Kavli Institute for Neuroscience, Yale University School of Medicine, New Haven, Connecticut 06510, USA. [2]Graduate Program in Areas of Basic and Applied Biology, Abel Salazar Biomedical Sciences Institute, University of Porto, Porto, Portugal. [3]Graduate Program in Neuroscience, Croatian Institute for Brain Research, University of Zagreb School of Medicine, Zagreb, Croatia. [4]Department of Biostatistics, Virginia Commonwealth University, Richmond, Virginia 23298, USA. [5]Yale Center for Genome Analysis, Yale University School of Medicine, New Haven, Connecticut 06510, USA. [6]Department of Pathology, Yale University School of Medicine, New Haven, Connecticut 06510, USA. [7]Clinical Brain Disorders Branch, National Institute of Mental Health, National Institutes of Health, Bethesda, Maryland 20892, USA. [8]The Lieber Insitute for Brain Development, Johns Hopkins University Medical Center, Baltimore, Maryland 20892, USA.

* These authors contributed equally to this work.

Correspondence:

Nenad Sestan, MD, PhD

E-mail: nenad.sestan@yale.edu

Lab website: www.sestanlab.org

SUMMARY

Our understanding of genetic mechanisms governing human brain development and their relevance to both human evolutionary specializations and the pathogenesis of brain disorders is hindered by a lack of comprehensive data on the spatiotemporal organization of the human brain transcriptome. Here we report the genome-wide, exon-level transcriptome analysis of 1,316 tissue samples from 16 brain regions, comprising the cerebellar cortex, mediodorsal nucleus of the thalamus, striatum, amygdala, hippocampus, and 11 areas of the neocortex, from both hemispheres of postmortem human brains. We also performed genome-wide genotyping for all specimens. Our data span from embryonic development to adulthood and represent both genders and multiple ethnicities. We found that approximately 82% of protein-coding genes are expressed above background in the sampled regions, and over 94% of these are differentially regulated across regions and/or time. The majority of these spatial and temporal changes in gene expression and alternative exon usage occurred before birth, followed by a progressive increase in the similarity between regional transcriptomes across postnatal development. Our analyses also identified novel spatiotemporal patterns of gene expression and alternative exon usage, gender differences in gene transcription, expression trajectories of disease-related genes, and networks of co-regulated transcripts associated with specific neurobiological processes. This dataset provides a public resource and new insights into the transcriptional foundations of human brain development, evolution, and dysfunction.

INTRODUCTION

The development of the human brain is a complex and precisely regulated process that unfolds over a protracted period of time[1-5]. Human-specific features of this process, especially the ways in which highly complex neural circuits of the cerebral cortex form, are likely to be important factors in the evolution of human specializations[5-10]. However, in addition to giving us remarkable cognitive and motor abilities, the formation of intricate neural circuits may have also increased our susceptibility to neuropsychiatric and neurodegenerative disorders[4,11-15]. Furthermore, substantial evidence suggests that the symptoms and progression of many brain disorders are dramatically influenced by genetic and developmental processes that define regional cell phenotypes and connectivity[16,17]. Thus, understanding the spatiotemporal dynamics and functional organization of the brain transcriptome is essential to teasing out the keys to human development and evolution as well as our increased susceptibility to certain brain disorders.

Most transcriptome studies of the developing brain have been restricted to rodents, and those performed in humans and non-human primates have included relatively small sample sizes and predominantly focused on few regions or developmental time points[18-23]. Because many prominent features of human brain development significantly diverge from those of well-characterized model organisms, the translation of knowledge across species is difficult, and it is likely that many underlying genetic processes have gone undetected[6,7,10,24,25]. In this study, we have taken a genome-wide approach to analyze the human transcriptome at single-exon resolution with 1.4 million probe sets in 16 brain regions, representing both genders and multiple ethnicities, across pre- and postnatal development, including adolescence, and adulthood. We also generated genome-wide genotype data for 2.5 million single nucleotide polymorphisms (SNPs) and copy number variants (CNVs) for each specimen. Our analyses of the data revealed features of the human brain transcriptome such as: spatiotemporal expression dynamics of individual and functionally related groups of genes; differential alternative exon usage; gender-specific expression patterns; and organization of the transcriptome into functional modules. We also profiled developmental trajectories of genes linked to autism and schizophrenia and important neurodevelopmental processes. This study is part of the Transcriptional Atlas of Human Brain Development Project designed to generate a comprehensive public resource on the transcriptome and epigenome of the developing human brain. The dataset presented here provides immediate

research opportunities and a wealth of information not previously available to the scientific community.

RESULTS

Study design and tissue processing

Brain development is a highly dynamic process during which different regions undergo distinct maturational changes. Moreover, transient brain structures arise and disappear during specific developmental periods[1,2]. Thus, it was crucial that multiple regions and major developmental time points were analyzed to allow for the identification of temporally and spatially specific transcriptional changes. We created a 15-period classification system based on age and major developmental milestones (Table 1; see Supplementary Information for details), particularly emphasizing the timing of specific neurodevelopmental events in the cerebral cortex, a structure that is central to the most distinctive traits of human cognition. We then analyzed multiple brain specimens per period to mitigate the effects of individual variations (Supplementary Table 1).

We also designed a structural ontology of 16 brain regions (Table 2), which were selected based on functional importance and accessibility for macrodissection. The ontology included several transient prenatal structures and the immature and mature forms of the cerebellar cortex (CBC), mediodorsal nucleus of the thalamus (MD), striatum (STR), amygdala (AMY), hippocampus (HIP), and cerebral neocortex (NCX) (Supplementary Figs. 1 and 2). We divided the NCX into 11 areas, including the prospective and mature primary motor and sensory (somatosensory, auditory, and visual) areas as well as the association areas of the prefrontal cortex (PFC), parietal cortex, and temporal cortex, which are involved in higher cognitive processes such as abstract thinking, decision-making, face recognition, speech, and language. Whenever possible, each region or area was sampled from both sides of the brain to generate biological replicates within an individual. We used standardized tissue dissection and processing methods performed by the same individuals and implemented a dissection scoring (DS) system to monitor the consistency between individual tissue samples (see Supplementary Information for details).

Brain tissue was obtained from largely clinically unremarkable donors of both genders and multiple ethnicities (Fig. 1a, b) (see Supplementary Information for details and metadata). All specimens were collected with approval of institutional review boards and informed consent. We recorded all available anonymous donor history and the postmortem interval (PMI) and measured

brain pH (Supplementary Table 1). We also generated genome-wide genotyping data from each donor for 2.5 million SNPs using Illumina Human Omni 2.5-Quad Bead Chips, which enabled us to corroborate ethnic background, and performed CNV analysis to identify genomic structural variants (see Supplementary Table 2 and Supplementary Information for details). Only specimens (N=57, including 33 with both hemispheres) with no signs of chromosomal or large-scale genomic abnormalities were included in the study (Fig. 1c). Demographic and quality control characteristics of the analyzed specimens were as follows: age, 5.7 post-conceptual weeks (PCW) to 84 years (Y); gender, 30 males and 27 females; PMI, 12.54±10.33 hours; pH, 6.45±0.33.

Generation and quality assessment of transcriptome data

Transcriptional profiling was performed using total RNA extracted from pulverized frozen tissue samples (Supplementary Methods). RNA quality was evaluated by determining the RNA integrity number (RIN) for each sample (mean=8.87±0.91 SD); only those with a RIN above 5 were processed (Fig. 1d). We used the Affymetrix GeneChip Human Exon 1.0 ST Array platform, which features comprehensive coverage of the human genome, with 1.4 million probe sets that assay exon expression across the entire transcript, thereby providing redundancy and increasing confidence in estimates of gene-level expression and differential expression (DEX) across tissue samples, time points, and between genders. In addition, exon-level profiling allows analysis of differential exon usage (DEU) and discovery of alternative isoform expression and splicing.

To control the quality of chip data we evaluated the presence of spatial artifacts and the degree of mRNA hybridization uniformity (see Supplementary Information and Supplementary Figs. 5 and 6 for details and methods). Low-quality chips identified by these quality control measures were excluded from further analysis and/or re-tested (N=20). To control for the impact of various confounding factors on the quantity, quality, and transcriptional profile of RNA, we computed correlations between gene expression and the following variables: PMI, pH, and RIN. Of these factors, PMI and RIN showed a very weak anticorrelation and correlation, respectively, with the number of expressed genes (Spearman correlation, r = -0.298 and 0.263, respectively; Supplementary Fig. 7), indicating that collected tissue samples are suitable for profiling the transcriptome.

To evaluate technical reproducibility, we assessed for possible batch effects by processing the same set of RNA samples at the two testing sites and calculating the correlations. To evaluate

biological reproducibility, we calculated the correlations between the same regions collected from different individuals of the same period. The correlations were high for both technical (Spearman correlation, r^2=0.967) and biological replicates (r^2=0.939), reinforcing the validity of our approach and data. Samples identified as outliers were re-processed and/or excluded from the study (see Supplementary Information for details). A total of 1,316 samples (out of 1,376) passed the quality control steps and were included in this study (Supplementary Table 3 and 4).

We performed principal component analysis (PCA) and multi-dimensional scaling (MDS) to identify key factors within the multi-dimensional transcriptome data set. Both analyses revealed first that age accounted for more variance in the data than any other tested variable (Supplementary Fig. 8 and 9). Secondly, they also revealed a substantial distinction between the NCX (in which 11 areas are clustered) and other regions (AMY, CBC, HIP, STR and MD) (Supplementary Figs. 8 and 9, and data not shown). Together, these findings corroborate our data and classification system. For complete details of tissue specimens and quality control assessments, see the Supplementary Information available online with this article.

Global gene-level analysis of the transcriptome

After quality control metrics were assessed, we performed a global analysis of gene expression by performing quantile normalization and summarizing the core probe set data into gene-level information. The dynamic spatiotemporal nature of gene regulation requires criteria for defining expressed genes that are only expressed in a narrow developmental window. Therefore, we defined an "expressed gene" as a gene with a mean detection above background (DABG) P <0.01 and log2-transformed expression value >6 in any one or more of the sampled regions/areas, at one or more time periods (see Supplementary Information for details). Out of 17,641 core transcripts, we found 14,526 (82.3%) protein-coding genes to be expressed in at least one brain region and period (Fig. 2a). In the NCX, 13,751 (77.9%) genes were expressed (Fig. 2b). To determine how many of these genes were spatially or temporally regulated, we used a conservative statistical threshold, i.e. a false discovery rate (FDR) q-value cutoff of 0.01 with a minimum 2-fold difference in expression between brain regions/areas or periods. We found that 9,482 genes (65.3% of expressed genes) were spatially DEX between any two brain regions within at least one period. Within NCX, a much smaller number, 2,560 (18.6%), were DEX among the 11 areas. The detection of spatially DEX genes was not significantly impacted by variations in DS (Spearman correlation, r = -0.214;

Supplementary Fig. 10), indicating that identified DEX genes reflect biological differences between analyzed regions.

In contrast to spatially DEX genes, we found 13,666 (94.1%) and 12,255 (89.1%) genes to be temporally DEX between any two periods across the brain regions and NCX areas, respectively. Furthermore, 9,422 (64.9%) and 2,555 (18.6%) of expressed genes were both spatially and temporally DEX in the brain and NCX, respectively, indicating that a majority of spatially DEX genes are also temporally regulated. These results suggest that gene expression patterns with spatial specificity tend to be transient. For instance, a majority of genes expressed in the NCX (8,570 or 62.3%) were temporally DEX across fetal development (periods 3-7), in contrast to 732 (5.3%) and a mere 83 (0.06%) during postnatal development (periods 8-12) and adulthood (periods 13-15), respectively. Together, these analyses show that the vast majority of brain-expressed protein-coding genes are temporally, and to a lesser extent, spatially regulated, revealing a highly dynamic transcriptional profile of human brain development.

Transcriptional architecture of the developing and adult human brain

To assess the relatedness of different tissue samples based on their expression profiles, we calculated correlation matrices of pair-wise comparisons between regions (Fig. 2c) and NCX areas (Fig. 2d). We performed unsupervised hierarchical clustering during fetal development (periods 3–7), postnatal development (periods 8-12), and adulthood (periods 13–15). We limited this spatial DEX analysis to periods 3-15, when regions/areas of interest are well-defined using equivalent criteria and can be consistently followed across time. We observed strong clustering of NCX, HIP, and AMY specifically during postnatal development and adulthood, indicating that transcriptional differences among these regions are most pronounced during human fetal development. Clustering of NCX areas based on correlations of their transcriptional profiles showed dynamic changes across development (Fig. 2d). In fetal samples, we found clustering of PFC areas (OFC, DFC, MFC, VFC) and primary motor-sensory cortex (M1C, S1C), which occupy the anterior half of the NCX, and separate clustering of the parietal-temporal perisylvian areas (IPC, A1C, STC) in the posterior NCX. Notably, there was a developmental increase in correlation between all NCX areas sampled except V1C, indicating that V1C maintains a transcriptional profile that is distinct from other NCX areas throughout pre- and postnatal development.

To gain insight into the underlying regional transcriptional differences, we searched among spatially DEX genes for those that are selectively enriched or restricted in only one of the regions, irrespective of their temporal regulation (Supplementary Table 5). We also searched for genes selectively enriched in the NCX, HIP, and AMY because of their functional relationship and strong clustering based on their transcriptome profiles (Fig. 2c). The CBC showed the greatest number of regionally selectively enriched genes, with 478 (5.04%) of 9,482 genes spatially DEX (Supplementary Table 5). In contrast, the number of genes highly enriched in the other regions was lower: NCX (42; 0.44%), HIP (39; 0.41%), AMY (2; 0.02%), STR (129; 1.36%), and MD (201; 2.12%). Among the NCX genes, several transcription factors that have been previously implicated in the development of NCX circuits in mice, such as *SATB2*[26,27], *SOX5*[28,29], and *TBR1*[30], were present, suggesting that the expression patterns and likely the underlying function of at least some of the regionally-enriched human genes that we identified are conserved in mammals.

Gene-level gender differences in transcriptional profiles

Gender differences play an important role in brain development and are a risk factor for several brain disorders, such as autism and depression[31]. Previous studies have revealed gender differences in gene expression in a few regions of the postnatal and adult human brain, including the dorsolateral PFC[32]. Our data set allowed us to compare gene expression between female and male brains in multiple regions throughout development and adulthood. Using a conservative statistical threshold (FDR <0.01 with >2-fold difference), we found that the largest gender differences were attributable to constant prenatal and postnatal expression of the Y chromosome genes *PCDH11Y*, *RPS4Y1*, *USP9Y*, *DDX3Y*, *NLGN4Y*, *UTY*, *EIF1AY*, and *ZFY* in males (Fig. 3), similar to the previous finding in the postnatal developing PFC[32]. Interestingly, the expression levels of the orthologous X-chromosome genes (*PCDH11X*, *RPS4X*, *USP9X*, *DDX3X*, *NLGN4X*, *UTX*, *EIF1AX*, and *ZFX*) did not significantly differ between genders ($P>0.05$). Among gender-specific genes, *PCDH11Y* exhibited the most notable changes in regional and temporal expression patterns. Both exon array and qRT-PCR validation data demonstrated that *PCDH11Y* was selectively down-regulated in CBC during postnatal development and adulthood but remained well-expressed in other regions (Supplementary Fig. 11). *PCDH11Y* encodes a protocadherin cell-surface adhesion molecule that has undergone positive selection during human evolution and has been linked to handedness and psychosis[33]. While sharp gender differences in gene expression across

development are largely attributable to the Y chromosome genes, we also found that a number of X chromosome and autosomal genes exhibited spatially- and temporally-restricted gender differences in expression (Supplementary Table 6). For example, *LOC554203*, a functionally uncharacterized transcript, and *S100A10* (also called p11), which has been linked to depression[34], are selectively up-regulated in several brain regions/areas and MFC, respectively, in the fetal female brain (Supplementary Table 6). Overall, we found specific regional and temporal differences in gender-specific gene expression that may be related to gender differences in brain maturation and organization.

The developing human brain transcriptome is organized into distinct modules

Analysis of differential gene expression does not convey all of the biological information embedded in multi-dimensional transcriptome data sets. To expand upon our analyses, we performed weighted gene co-expression network analysis to identify modules of co-regulated genes[35,36]. We identified 25 modules corresponding mostly to specific spatiotemporal patterns and functional themes (Fig. 4a). A list of genes comprising the modules and functional annotations are provided in Supplementary Table 7. Among modules corresponding to specific spatial and temporal expression patterns, module M8 consisted of 29 genes with a common developmental trend that exhibits highest levels in early fetal NCX and HIP (period 3) and then progressively declines with age until infancy (period 9) (Fig. 4b, c). In contrast, module M15 contained 114 genes exhibiting changes in the opposite direction in the NCX, HIP, AMY, and STR. The levels are lowest during early fetal development and then gradually increase with age until peaking during infancy (Fig. 4e, f). We used DAVID (http://david.abcc.ncifcrf.gov) to assign functional enrichment scores to the genes within each module. Of the 29 genes in M8, 12 encode transcription factors (Bonferroni adjusted $P=5.6\times10^{-6}$), 7 of which are involved in neuronal differentiation (Bonferroni adjusted $P=3.7\times10^{-2}$) (Supplementary Table 7). Genes with the highest degree of connectivity within a module are termed hub genes and are expected to be functionally important within the module. Hub genes of the M8 transcription factor module include *EMX1*, *FEZF2*, *FOXG1*, *NEUROD2*, *NEUROD6*, and *TBR1* (Fig. 4d), which previously have been functionally implicated in the development of neural circuits in the mouse NCX or HIP[30,37,38]. Furthermore, *FOXG1* variants have been linked to Rett syndrome and mental retardation[38]. In contrast to M8, M15 is enriched in genes encoding ionic channels (Bonferroni adjusted $P=8.6\times10^{-}$

[8]) and genes functioning in synaptic transmission (Bonferroni adjusted $P=3.6\times10^{-6}$) (Supplementary Table 7). Sequence variants in two hub genes, *GDA* and *HTR2A* (Fig. 4g), have been linked to major depression[39] and to schizophrenia and affective disorders[40], respectively.

We also identified two large modules (M20 and M2) composed of genes that appear to be simultaneously co-regulated across all sampled regions and to have opposite developmental trajectories. M20 contains 3,081 genes that exhibit highest levels during embryonic and early fetal periods and then gradually decline with age until early childhood (Supplementary Fig. 12). In contrast, M2 contains 2,773 genes that are expressed at lowest levels during embryonic and early fetal periods and then gradually increase before birth until peaking around early childhood (Supplementary Fig. 13). The time point at which the trajectories of M20 and M2 cross and exhibit very dramatic expression shifts is just before birth during the late-fetal period (Supplementary Figs. 12 and 13), indicating that the perinatal period in humans is associated with dynamic changes in gene expression. Functional annotation indicates that M20 is enriched with genes encoding zinc finger proteins (Bonferroni adjusted $P=3.6\times10^{-70}$) and transcription factors (Bonferroni adjusted $P=2.1\times10^{-45}$), including many ZNF and SOX family members. M2 consists of genes encoding membrane proteins (Bonferroni adjusted $P=1.8\times10^{-25}$) and genes involved in calcium signaling (Bonferroni adjusted $P=1.8\times10^{-11}$), synaptic transmission (Bonferroni adjusted $P=3.4\times10^{-8}$), and neuroactive ligand-receptor interaction (Bonferroni adjusted $P=5.2\times10^{-9}$), reflecting functional processes involved in maturation of the postnatal brain (Supplementary Table 7). Our validations using qRT-PCR confirmed expression trajectories of several genes within the M2 and M20 modules (Supplementary Figs. 12 and 13).

We identified additional modules with clear spatiotemporal specificity, such as M9 (MD), M19 (CBC), M23 (STR), M16 (NCX, HIP, CBC), and M18 (NCX) (see Supplementary Table 7, and Supplementary Figs. 14, 15, and 16 for details and validation), as well as modules that exhibited no obvious spatiotemporal expression patterns but were enriched in genes associated with cell cycle (M1), cytoskeleton (M3), extracellular matrix (M5), and sensory processing and RNA splicing (M12) (Supplementary Table 7). Overall, our findings show that the developing human brain transcriptome is organized into modules of coordinated genes associated with distinct spatiotemporal expression patterns and biological processes.

Global analysis of differential alternative exon usage

Our genome-wide exon-level expression data provides an opportunity to investigate the dynamics of alternative exon usage, an important mechanism for generating transcript diversity in the developing human brain. Using conservative criteria, FDR <0.01 with a minimum 2-fold splice index difference between at least two regions or periods, we found that 12,895 of 14,526 (88.8%) expressed genes exhibit DEU across sampled regions (0.1%), periods (40.9%), or both (47.8%) (Fig. 5a). Of 13,751 genes expressed in NCX, 88.3% exhibit DEU across sampled areas (<0.01%), periods (71.1%), or both (17.1%) (Fig. 5b). The regulation of DEU also varied dramatically across time, with the vast majority of expressed genes (78.6%) exhibiting temporal DEU across fetal development (periods 3-7), while 32.1% and 29,4% were temporally regulated across postnatal development (periods 8-12) and adulthood (periods 13-15), respectively. These findings suggest that the temporal regulation of DEU is more prevalent during fetal development and declines as the brain matures.

We used our data set to analyze spatial and temporal differences in alternative exon usage in *ANKRD32*, a gene previously shown to express an alternative variant in the late mid-fetal frontal cortex. Specifically, the longer isoform (*ANKRD32a*) is equally expressed across NCX areas, while the exons associated with the shorter isoform (*ANKRD32b*) are highly enriched in the prefrontal areas[22]. However, it is not known if this expression pattern of the *ANKRD32* isoforms is restricted to the late mid-fetal frontal cortex. We found that *ANKRD32a* is consistently expressed across early fetal, late mid-fetal, and adult NCX areas (Fig. 5c, d). In contrast, *ANKRD32b* exhibited significant differences in expression between areas of the early fetal and mid-fetal NCX (One-way ANOVA, $P=1.3\text{x}10^{-5}$ and $P=1.9\text{x}10^{-7}$, respectively). Using primers against the 5'UTR of the short isoform[22] to perform qRT-PCR, we confirmed that *ANKRD32b* is restricted to the late mid-fetal frontal cortex in an independent data set. We found that *ANKRD32b* is expressed in a gradient along the anterior-posterior axis with highest expression in OFC and lowest in M1C. We also identified a shift in the expression of *ANKRD32b* during early fetal periods 3 and 4, where the shorter isoform is most highly enriched in the ITC and, to a lesser extent, in the STC (One-way ANOVA $P=1.3\text{x}10^{-5}$, followed by Tukey's pair-wise test; see Supplementary Table 8). These spatiotemporal expression patterns disappear after birth, when only *ANKRD32a* is present in NCX. Together, these findings illustrate how specific alternative transcripts can be transiently and differentially expressed between NCX areas during a narrow developmental window.

Expression trajectories of disease-related genes

One of the most important advantages of a spatially and temporally comprehensive transcriptome data set is to generate expression profiles for individual genes and gene families of interest. This is particularly important for tracking the developmental trajectories of genes whose variants have been implicated in neuropsychiatric disorders such as autism and schizophrenia. These disorders affect the most distinctive aspects of human cognition while the underlying neurodevelopmental alterations remain poorly understood[11-15,41-43]. Here, we chose to profile spatiotemporal expression patterns and identify correlated transcripts of a number of genes whose variants have been linked to these two disorders (see Supplementary Information and Supplementary Tables 9 and 10 for details). We observed many distinct and dynamic expression patterns, especially between NCX areas. For instance, *CNTNAP2*, which encodes a neurexin family protein implicated in autism, is highly enriched in the areas of the fetal OFC and DFC, as previously reported[21,22]. Here we confirmed and extended these findings using a different dataset. We found that expression levels of *CNTNAP2* suddenly increase in other cortical areas during early infancy (period 8), after which it remains expressed in all NCX areas (Fig. 6a). We also found that *CNTNAP2* is dynamically regulated in subcortical regions during development. Likewise, *MET*, which encodes a hepatocyte growth factor receptor, is also linked to autism[43] and exhibits a partially overlapping but distinct NCX areal expression pattern (Fig. 6b). *MET* is highly enriched in the early mid-fetal ITC and then increases in the surrounding temporal-occipital areas and the OFC, where it remains enriched throughout development. Interestingly, these developmental and areal patterns of *MET* expression have not been observed in rodents, indicating inter-species differential expression[21,44].

Striking expression patterns were also observed for several genes linked to schizophrenia, including *TCF4* and *NRGN* [41]. For instance, we found that *TCF4*, which encodes a transcription factor also affected in the neurodevelopmental disorder Pitt-Hopkins syndrome[42], is highly enriched across NCX areas, HIP, and AMY during prenatal periods, and then declines sharply after birth (Fig. 6c). *NRGN*, which encodes a postsynaptic protein kinase substrate, is highly expressed in all NCX areas starting after birth and progressively increases in expression until late childhood (Fig. 6d). These examples illustrate the spatiotemporal expression patterns of a few genes linked to autism and schizophrenia, which may yield insights into which particular human brain circuits and what particular periods in development may be affected by alterations in the

function of these genes.

To gain insight into biological functions of a number of genes commonly associated with autism (*FMR1*, *NLGN4X*, *NRXN1*, *SHANK2*, *NLGN3*, *CNTN4*, *CNTNAP2*, *SYNGAP1*, *DLGAP2*, *EN2*, and *MET*) and schizophrenia (*PRSS16*, *PGBD1*, *NRGN*, *NOTCH4*, *PDE4B*, *TCF4*, *DRD4*, *DAOA*, *TPH1*, *HTR2A*, *MDGA1*, *APOE*, *DISC1*, *AKT1*, *PLXNA2*, and *SRR*) in the developing human brain, we identified other genes with significantly correlated spatiotemporal expression profiles (Supplementary Tables 9 and 10; see Supplementary Information for details on gene selection and methods). Functional annotation suggested that the genes from our data set most highly correlated with autism-related genes are predominantly associated with neuron projection (Bonferroni Bonferroni adjusted $P=3.8 \times 10^{-14}$), phosphoproteins (Bonferroni adjusted $P=5.6 \times 10^{-8}$), membrane proteins (Bonferroni adjusted $P=2.7 \times 10^{-11}$), synapse (Bonferroni adjusted $P=1.2 \times 10^{-14}$), and synaptic transmission (Bonferroni adjusted $P=3.6 \times 10^{-10}$). Likewise, genes from our data set most highly correlated with schizophrenia-related genes are mainly associated with membrane proteins (Benjamini adjusted $P=1.1 \times 10^{-3}$), phosphoproteins (Bonferroni adjusted $P = 2.3 \times 10^{-3}$), transcription regulation (Bonferroni adjusted $P=4.8 \times 10^{-3}$), and zinc finger proteins (Bonferroni adjusted $P=1.2 \times 10^{-2}$). Together, these analyses provide examples of how our data set can be used to generate spatiotemporal expression trajectories and lists of genes correlated with disease-related genes that may not be revealed using transcriptome data from model organisms.

Developmental trajectories of human neurobiological processes

Technical and ethical issues have limited the in-depth study of biological processes in the developing human brain. One of the most important applications for the data set reported here is the assessment of regional differences and developmental trajectories of human neurobiological processes by inference from the expression patterns of individual genes or groups of known genes with related biological functions. To test the viability and accuracy of this strategy, we analyzed several developmental trajectories for which we could compare our gene expression data with independently generated, non-transcriptome data sets from the developing human brain. We first analyzed the expression of a single gene, *DCX*, which encodes a brain-specific microtubule-associated protein expressed in neural progenitor cells and migrating immature neurons[45]. Recently, immunohistochemistry data was generated for DCX in the hippocampus across the

lifespan from 0 to 100 years[45]. In our transcriptome data set, *DCX* is expressed as early as 5.7 PCW in the hippocampus, and its expression progressively increases until early mid-fetal development (period 5) and then gradually declines with age until early childhood (period 10), a profile that is consistent with its role in neurogenesis and neuronal migration (Fig. 7a). Moreover, this developmental trajectory of *DCX* expression is remarkably reminiscent of the reported changes in the density of DCX-immunopositive cells in the postnatal human hippocampus.

Next, we analyzed the trajectories of groups of functionally related genes for dendrite development and synpatogenesis (see Supplementary Information for details on gene selection and methods). Our gene annotation-based trajectories for dendrite development (*MAP1A*, *MAPT*, *CAMK2A*) and excitatory synaptogenesis (*SYP*, *SYPL1*, *SYPL2*, *SYN1*) in the dorsolateral PFC closely parallel, and were highly correlated with, the developmental patterns observed in independently generated data on the growth of basal dendrites of layers 3 and 5 pyramidal neurons in the human PFC [46,47] (Spearman correlation, $r = 0.818$ for layer 3 and $r = 0.714$ for layer 5; Fig. 7b) and synaptic counts in the postnatal PFC[48] (Spearman correlation, $r = 0.936$; Fig. 7c), respectively. Steep increases in both dendritic development and synaptogenesis occurred between late-midfetal and late infancy, indicating that a considerable portion of these two processes occurs before birth and reaches a plateau around late infancy.

We also profiled the expression of genes associated with distinct subclasses of cortical GABAergic interneurons for which we have generated immunohistochemical validation data (Supplementary Fig. 17). For instance, our expression trajectories of markers of several classes of cortical GABAergic inhibitory interneurons (i.e., *CALB1, CALB2, NOS1, PVALB*, *VIP*) showed that the onset of their expression and maturational trajectories vary widely in the human NCX. Consistent with previously published data and our immunohistochemical analysis[49] (Supplementary Fig. 17), *CALB2* (also known as calretinin) was the first of these genes to appear in the cerebral wall as early as period 1, while the expression of other markers (*CALB1, NOS1, VIP* and *PVALB*) followed different temporal patterns. Of the analyzed genes, parvalbumin (*PVALB*) exhibited the most protracted developmental trajectory, not reaching maximum level until around adolescence (Supplementary Fig. 17), notably, a developmental period during which the symptoms of schizophrenia and other neuropsychiatric disorders typically arise[11-15]. Intriguingly, alterations in PVALB-immunopositive interneurons have been reported in patients with schizophrenia and seizures[15,50]. Together, the examples presented here demonstrate how these transcriptome data can

be used to assess the onset and the developmental trajectories of major neurobiological processes and cell types in the human brain.

DISCUSSION

We report the generation and analysis of a comprehensive genome-wide exon-level transcriptome and corresponding genotyping dataset covering multiple brain regions and NCX areas. Tissue collection, dissection and processing as well as all data generation procedures were performed using standardized protocols and were subjected to extensive quality control measures to ensure data consistency and reproducibility. The generated data set covers nearly the entirety of human brain development and adulthood, from the embryonic period through late adulthood, and was subjected to multiple validation procedures. The data generated thus far expands current knowledge of the transcriptional processes that govern human brain development and provide immediate opportunities for a variety of further investigations. Data from this study are publicly available via multiple avenues, including a searchable database (www.humanbraintranscriptome.org). These data will also provide opportunities for comparison with other existing and forthcoming large-scale gene expression and transcriptome data sets generated from different human conditions and model organisms.

Our data set provides a comprehensive resource for the study of human spatiotemporal gene expression, differential isoform expression, co-regulated transcripts, multiregional left-right transcriptional asymmetry, and effects of genetic variations on gene expression and splicing. We presented selected findings and examples of how this data set can be mined at both the gene- and exon- level to uncover features of the developing human brain transcriptome pertinent to a wide range of interests and a variety of perspectives. We found that approximately 82% of genes are expressed in the sampled regions and over 94% of these are differentially regulated, predominantly in the form of temporal regulation of gene expression and alternative exon usage. By multiple measures, the prenatal human brain exhibited the most dynamic spatiotemporal regulation of the transcriptome, followed by the postnatal brain through adolescence, with the adult characterized by the least number of genes DEX across regions, NCX areas, or time periods. Wealso also found a progressive increase in correlation of the transcriptome across NCX areas and between cellularly and functionally related structures (e.g., NCX, HIP, AMY) during development (Fig. 2). Furthermore, our analysis of co-expressed gene networks also identified large modules comprised

of genes that exhibit opposite trajectories and a reversal in gene expression across multiple regions just before birth (late-fetal period). We speculate that these findings likely reflect several underlying phenomena and features of human brain structure and development. One such feature is a general trend of pronounced transcriptional differences during embryonic and fetal development, when specific neural circuits are being established, followed by an increased correlation between functionally related regions and NCX areas in the postnatal and adult brain. Furthermore, perinatal reversals in expression of a large number of genes may reflect intrinsic changes in developmental processes between fetal and postnatal development as well as effects of early experience and environment on brain development.

We also demonstrated how this data set can be used to identify novel spatial and temporal patterns of alternative exon usage. Specifically, we showed that an alternative isoform of *ANKRD32* forms a transient graded expression pattern in the PFC during mid-fetal development. The great majority of genes and alternative isoforms analyzed in this study have not previously been characterized, emphasizing how little is known about genetic mechanisms in the developing human brain. Our analysis confirmed and expanded on previous findings on gender-specific differences across different brain regions and spanning almost the entire period of brain development. We also demonstrated the accuracy and usefulness of the data in profiling spatial differences and developmental trajectories of genes related to specific neurobiological processes and brain disorders, most of which likely would not be evident in transcriptome data generated from model organisms. Importantly, as more data sets are generated from healthy and diseased brains of humans and other species throughout development, and as we expand our understanding of neurobiological processes and genetic alterations associated with human disease, it will be possible to uncover additional insights into the transcriptional foundations of human brain development, evolution, and dysfunction.

METHODS SUMMARY

A summary of the methods, together with a full description of tissue acquisition and processing, data generation and analyses, and associated references can be found in Supplementary Information.

Supplementary Information is linked to the online version of the paper at www.nature.com/nature.

Accession code. National Center for Biotechnology Information (NCBI) Gene Expression Omnibus (GEO accession number GSE25219) and database of Genotypes and Phenotypes (dbGAP; accession number pending).

ACKNOWLEDGMENTS

We thank V. Imamovic, R. Johnson, P. Larton, S. Lindsay, S. Lisgo, B. Poulos, J. Rajan, D. Rimm, and R. Zielke for assistance with tissue acquisition, D. Singh for technical assistance, M. Judas, I. Kostovic and Z. Petanjek for help in designing developmental periods and providing Golgi measurements, N. Carriero and R. Bjornson for creating a sample tracking database, P. Levitt for suggesting the ITC, D. Karolchik and A. Zweig for help in creating tracks for the UCSC Genome browser. We also thank S. Anderson, A. Beckel-Mitchener, M. Freund, M. Gerstein, D. Geschwind, M. Hawrylycz, T. Insel, M. Judas, K. Kaila, J. Knowles, I. Kostovic, E. Lein, P. Levitt, J. Noonan, J. Rubenstein and members of the Sestan laboratory for constructive discussions. Human tissue was obtained from several sources including the NICHD Brain and Tissue Bank for Developmental Disorders at the University of Maryland, Baltimore, MD, and the Joint MRC Wellcome Trust Human Developmental Biology Resource (http://www.hdbr.org) at the IHG, Newcastle upon Tyne, UK. Support for pre-doctoral fellowships was provided by the China Scholarship Council (Y.Z.), the Portuguese Foundation for Science and Technology (A.M.M.S.), and the Samsung Scholarship Foundation (Y.S.), and. This work was supported by grants from the US National Institutes of Health (MH081896, MH089929, NS051869), Kavli Foundation, NARSAD, and the James S. McDonnell Foundation Scholar Award (N.S.).

AUTHOR CONTRIBUTIONS

H.Y.K., Y.I.K., A.M.M.S., M.P., K.A.M., G.S., Y.S., M.B.J., Z.K., S.F., S.U. and N.S. performed and analyzed the experiments. F.C., Y.Z., X.X., M.L., T.G., and M.R. analyzed the data. D.R.W., S.M., T.H.H., M.R., J.E.K. and N.S. examined and interpreted the results. A.V., T.H.H., A.H., J.E.K., and N.S. participated in tissue procurement and performed neuropathological examination. N.S. conceived and designed the study and wrote the manuscript, which all authors edited.

COMPETING FINANCIAL INTERESTS

The authors declare no competing financial interests.

TABLES

Table 1 | Periods of human development and adulthood as defined in this study.

Period	Description	Age
1	Embryonic	4≤ Age <8 Postconceptual weeks (PCW)
2	Early fetal	8≤ Age <10 PCW
3	Early fetal	10≤ Age <13 PCW
4	Early mid-fetal	13≤ Age <16 PCW
5	Early mid-fetal	16≤ Age <19 PCW
6	Late mid-fetal	19≤ Age <24 PCW
7	Late fetal	24≤ Age <38 PCW
8	Neonatal and early infancy	Birth≤ Age <6 Postnatal months (M)
9	Late infancy	6 M≤ Age <12 M
10	Early childhood	1≤ Age <6 Y
11	Middle and late childhood	6≤ Age <12 Y
12	Adolescence	12≤ Age <20 Y
13	Young adulthood	20≤ Age <40 Y
14	Middle adulthood	40≤ Age <60 Y
15	Late adulthood	60 Y ≤ Age

Table 2 | Ontology and nomenclature of analyzed brain regions and neocortical areas.

Period 1	Period 2	Periods 3 - 15
FC: Frontal cerebral wall	**FC**	**OFC**: Orbital prefrontal cortex
		DFC: Dorsolateral prefrontal cortex
		VFC: Ventrolateral prefrontal cortex
		MFC: Medial prefrontal cortex
		M1C: Primary motor (M1) cortex
PC: Parietal cerebral wall	**PC**	**S1C**: Primary somatosensory (S1) cortex
		IPC: Posterior inferior parietal cortex
TC: Temporal cerebral wall	**TC**	**A1C**: Primary auditory (A1) cortex
		STC: Posterior superior temporal cortex
		ITC: Inferior temporal cortex
OC: Occipital cerebral wall	**OC**	**V1C**: Primary visual (V1) cortex
HIP: Hippocampal anlage	**HIP**	**HIP**: Hippocampus
		AMY: Amygdala
VF: Ventral forebrain	**CGE**: Caudal ganglionic eminence	**STR**: Striatum
	LGE: Lateral ganglionic eminence	
	MGE: Medial ganglionic eminence	
DIE: Diencephalon	**DTH**: Dorsal thalamus	**MD**: Mediodorsal nucleus of thalamus
URL: Upper (rostral) rhombic lip	**URL**	**CBC**: Cerebellar cortex

FIGURE LEGENDS

Figure 1 | Demographics and genotyping of analyzed brain specimens and quality analysis of RNA samples. **a**, Gender distribution of specimens. **b**, Ethnicity distribution of specimens according to SNP genotypes. **c**, Number of CNVs per individual specimen distributed across genders and developmental periods. **d**, RNA integrity numbers for 1,316 tissue samples generated in this study.

Figure 2 | Global spatiotemporal properties of the human brain transcriptome at the gene-level. **a**, **b**, Venn diagrams show the numbers of total genes expressed, and spatially (pink) and temporally (blue) DEX genes across indicated (a) brain regions and (b) neocortical areas. Only genes with FDR <0.01 and a minimum 2-fold difference between at least two regions or two periods were considered to be spatially or temporally DEX, respectively. **c**, **d** Heat map matrix representations of pairwise gene expression correlations between 6 brain regions (c) or 11 neocortical areas (d) during fetal development (periods 3-7), postnatal development (periods 8-12), and adulthood (periods 13-15). Correlations were computed based on the averaged signal intensity level across specified periods, and clustered according to similarity using average linkage hierarchical clustering. The dendrograms relate regions/areas to one another.

Figure 3 | Global developmental gender differences in global gene expression. Box plots showing the averaged log2-transformed ratio of male and female gene expression across brain regions and NCX areas during fetal development (periods 3-7), postnatal development (periods 8-12), and adulthood (periods 13-15). The dashed line represents the cut-off at 2-fold difference. Each blue circle represents a gene with a minimum 2-fold difference in expression and FDR <0.01 in at least one of the regions. Y-chromosome (blue), X-chromosome (red), and autosomal genes (green) listed in parentheses do not exhibit significant global gender differences, but are significantly different (FDR <0.01) between genders only in a subset of regions and periods analyzed. Details on these genes are available in Supplementary Table 6.

Figure 4 | Gene co-expression networks and gene modules associated with specific spatiotemporal expression pattern or biological function. a, Dendrogram from gene co-expression network analysis of samples from periods 3 to 15. Modules of co-expressed genes are assigned colors and labeled with numbers. Details on the modules and list of genes involved are provided in the Supplementary Information. **b**, Heat map of genes in module M8 after a hierarchical clustering showing the spatiotemporal pattern of the module. The expression values for each gene are hierarchically arranged in the heat map, ordered first by brain regions, then by age, and last by NCX areas (OFC, DFC, VFC, MFC, M1C, S1C, IPC, A1C, STC, ITC, V1C). **c**, The spatiotemporal pattern of M8 was summarized using PCA for expression of genes in the module. The first principal component (PC1) was displayed along age, after being grouped and color-coded according to brain regions. The pattern was summarized by the smoothed curves of PC1 values. **d**, Co-expression network within module M8. The top 10 genes (hub genes), defined by the highest intramodular connectivity with the other genes, are highlighted in red. **e**,**f**,**g** are similar analysis for module M15 as **b**,**c**,**d**. Dashed lines in (c) and (f) represent division between periods, and the solid line represents the division between prenatal and postnatal development. Results for other modules are available in Supplemental Information.

Figure 5 | Differential alternative exon usage and isoform expression in the developing human brain. a, b, Venn diagrams show the numbers of spatial DEU genes (green) and temporal DEU (yellow) across indicated brain regions (a) or NCX areas (b). **c**, Identification of DEU across neocortical regions by exon array probeset-level expression data. Plotted are log2-transformed signal intensity levels (y-axis) for each probeset and its matching exons (x-axis) for gene *ANKRD32*. The location of isoform specific primers are depicted by blue (*ANKRD32a*) and green (*ANKRD32b*) arrows. **d,** qRT-PCR analysis of the long (blue bars) and short (green bars) *ANKRD32* isoforms (*ANKRD32a* and *ANKRD32b*, respectively) represented as relative gene expression levels (mean ± SEM). qRT-PCR data were analyzed by one-way ANOVA followed by Tukey's pair-wise test (Supplementary Table 8). NCX area was chosen as the ANOVA factor. **e**, Semi-quantitative PCR products are visualized by gel-electrophoresis analysis.

Figure 6 | Spatiotemporal expression trajectories of disease-related genes. a-d, Heat map matrix representations of dynamics in spatiotemporal expression of representative genes whose variants have been previously linked to (a, b) autism (*CNTNAP2, MET*) and (c, d) schizophrenia (*TCF4*, *NRGN*). The expression images display log2-transformed signal intensity across analyzed regions/areas and time periods using a heat map color scale, from low (blue) to high (red). The black line separates NCX areas from other brain regions.

Figure 7 | Expression-based profiling of developmental trajectories of neurobiological processes. **a**, Comparison between transcriptome-based trajectory for hippocampal *DCX* and independently generated immunohistochemical data set on density of DCX-positive cells in the postnatal and adult human hippocampal dentate gyrus[45]. Note that data on density of DCX-positive cells for the prenatal hippocampus was not available. **b**, Comparison between dendrite development trajectories for the DFC generated with our transcriptome data set and manually curated gene annotation (*MAP1A, MAPT, CAMK2A*) (blue) with independent data set on the development of basal dendrites of layer (L) 3 (red) and 5 (orange) pyramidal neurons in the developing human dorsolateral PFC generated using the Golgi method[46,47]. **c**, Comparison between transcriptome-based trajectories for the DFC generated with the manually curated synaptogenesis gene annotation (*SYP, SYPL1, SYPL2, SYN1*) (blue) and independent data set on density of dorsolateral PFC synapses (red) generated using electron microscopy starting with the late fetal period (period 6 in this study)[48]. We used PCA to summarize the expression pattern of multiple genes associated with the gene annotations in b and c. The first principle component (PC1), which accounts for the majority of variability in the data, was plotted against age to represent the developmental trajectory. Different datasets were scaled by $\frac{x-\mu}{\sigma}$. μ and σ are the mean and the standard deviation of values corresponding to the time periods for which both our gene expression and the independently obtained data were available. The density of DCX-immunopositive cells (a), the number of dendrites (b) and the density of synapse (c) were plotted in logarithmic scales.

REFERENCES

1 Bystron, I., Blakemore, C. & Rakic, P. Development of the human cerebral cortex: Boulder Committee revisited. *Nat Rev Neurosci* **9**, 110-122 (2008).
2 Kostovic, I. & Judas, M. Prolonged coexistence of transient and permanent circuitry elements in the developing cerebral cortex of fetuses and preterm infants. *Dev Med Child Neurol* **48**, 388-93 (2006).
3 Howard, B. M. et al. Radial glia cells in the developing human brain. *Neuroscientist* **14**, 459-473 (2008).
4 Rubenstein, J. L. Research Review: Development of the cerebral cortex: implications for neurodevelopmental disorders. *J Child Psychol Psychiatry*, doi: 10.1111/j.1469-7610.2010.02307.x (2010).
5 Hill, R. S. & Walsh, C. A. Molecular insights into human brain evolution. *Nature* **437**, 64-67 (2005).
6 Preuss, T., Cáceres, M., Oldham, M. & Geschwind, D. Human brain evolution: insights from microarrays. *Nat Rev Genet* **5**, 850-860 (2004).
7 Sherwood, C., Subiaul, F. & Zawidzki, T. A natural history of the human mind: tracing evolutionary changes in brain and cognition. *J Anat* **212**, 426-454 (2008).
8 Rakic, P. Evolution of the neocortex: a perspective from developmental biology. *Nat Rev Neurosci* **10**, 724-735 (2009).
9 Kriegstein, A., Noctor, S. & Martínez-Cerdeño, V. Patterns of neural stem and progenitor cell division may underlie evolutionary cortical expansion. *Nat Rev Neurosci* **7**, 883-890 (2006).
10 Molnár, Z., Métin, C., Stoykova, A., Tarabykin, V., Price, D. J., Francis, F., Meyer, G., Dehay, C. & Kennedy, H. Comparative aspects of cerebral cortical development. *Eur J Neurosci* **23**, 921-934 (2006).
11 Insel, T. Rethinking schizophrenia. *Nature* **468**, 187-193 (2010).
12 State, M. The genetics of child psychiatric disorders: focus on autism and Tourette syndrome. *Neuron* **68**, 254-269 (2010).
13 Crow, T. The 'big bang' theory of the origin of psychosis and the faculty of language. *Schizophr Res* **102**, 31-52, (2008).
14 Meyer-Lindenberg, A. & Weinberger, D. R. Intermediate phenotypes and genetic mechanisms of psychiatric disorders. *Nat Rev Neurosci* **7**, 818-827 (2006).
15 Lewis, D. A. & Levitt, P. Schizophrenia as a disorder of neurodevelopment. *Annu Rev Neurosci* **25**, 409-432 (2002).
16 Morrison, J. & Hof, P. Life and death of neurons in the aging brain. *Science* **278**, 412-419 (1997).
17 Subramaniam, S., Sixt, K., Barrow, R. & Snyder, S. Rhes, a striatal specific protein, mediates mutant-huntingtin cytotoxicity. *Science* **324**, 1327-1330 (2009).
18 Miska, E. A. et al. Microarray analysis of microRNA expression in the developing mammalian brain. *Genome Biol* **5**, R68, http://genomebiology.com/2004/5/9/R68 (2004).
19 Ip, B. et al. Investigating gradients of gene expression involved in early human cortical development. *J Anat* **217**, 300-311 (2010).
20 Sun, T. et al. Early asymmetry of gene transcription in embryonic human left and right cerebral cortex. *Science* **308**, 1794-1798 (2005).
21 Abrahams, B. et al. Genome-wide analyses of human perisylvian cerebral cortical patterning. *Proc Natl Acad Sci U S A* **104**, 17849-17854 (2007).
22 Johnson, M. B. et al. Functional and evolutionary insights into human brain development through global transcriptome analysis. *Neuron* **62**, 494-509 (2009).
23 Somel, M. et al. MicroRNA, mRNA, and protein expression link development and aging in human and macaque brain. *Genome Res* **20**, 1207-1218 (2010).
24 Mirnics, K. What is in the brain soup? *Nat Neurosci* **11**, 1237-1238 (2008).
25 Dehay, C. & Kennedy, H. Transcriptional regulation and alternative splicing make for better brains. *Neuron* **62**, 455-457 (2009).
26 Britanova, O. et al. Satb2 is a postmitotic determinant for upper-layer neuron specification in the neocortex. *Neuron* **57**, 378-392 (2008).
27 Alcamo, E. et al. Satb2 regulates callosal projection neuron identity in the developing cerebral cortex. *Neuron* **57**, 364-377 (2008).
28 Kwan, K. et al. SOX5 postmitotically regulates migration, postmigratory differentiation, and projections of subplate and deep-layer neocortical neurons. *Proc Natl Acad Sci U S A* **105**, 16021-16026 (2008).

29 Lai, T. et al. SOX5 Controls the sequential generation of distinct corticofugal neuron subtypes. *Neuron* **57**, 232-247 (2008).
30 Hevner, R. et al. Tbr1 regulates differentiation of the preplate and layer 6. *Neuron* **29**, 353-366, (2001).
31 Baron-Cohen, S., Knickmeyer, R. & Belmonte, M. Sex differences in the brain: implications for explaining autism. *Science* **310**, 819-823 (2005).
32 Weickert, C. et al. Transcriptome analysis of male-female differences in prefrontal cortical development. *Mol Psychiatry* **14**, 558-561 (2009).
33 Kalmady, S. & Venkatasubramanian, G. Evidence for positive selection on protocadherin Y gene in Homo sapiens: implications for schizophrenia. *Schizophr Res* **108**, 299-300 (2009).
34 Svenningsson, P. et al. Alterations in 5-HT1B receptor function by p11 in depression-like states. *Science* 311, 77-80 (2006).
35 Oldham, M. et al. Functional organization of the transcriptome in human brain. *Nat Neurosci* **11**, 1271-1282 (2008).
36 Zhang, B. & Horvath, S. A general framework for weighted gene co-expression network analysis. *Stat Appl Genet Mol Biol* **4**, Article17, doi: 10.2202/1544-6115.1128 (2005).
37 Chen, J., Rasin, M., Kwan, K. & Sestan, N. *Zfp312* is required for subcortical axonal projections and dendritic morphology of deep-layer pyramidal neurons of the cerebral cortex. *Proc Natl Acad Sci U S A* **102**, 17792-17797 (2005).
38 Ariani, F. et al. *FOXG1* is responsible for the congenital variant of Rett syndrome. *Am J Hum Genet* **83**, 89-93 (2008).
39 Perroud, N. et al. Genome-wide association study of increasing suicidal ideation during antidepressant treatment in the GENDEP project. *Pharmacogenomics J*, doi:10.1038/tpj.2010.70 (2010).
40 Serretti, A., Drago, A. & De Ronchi, D. HTR2A gene variants and psychiatric disorders: a review of current literature and selection of SNPs for future studies. *Curr Med Chem* **14**, 2053-2069 (2007).
41 Stefansson, H. et al. Common variants conferring risk of schizophrenia. *Nature* **460**, 744-747 (2009).
42 Blake, D. J. et al. TCF4, schizophrenia, and Pitt-Hopkins syndrome. *Schizophr Bull* **36**, 443-447 (2010).
43 Campbell, D. B. et al. A genetic variant that disrupts MET transcription is associated with autism. *Proc Natl Acad Sci U S A* **103**, 16834-16839 (2006).
44 Judson, M. C., Amaral, D. G. & Levitt, P. Conserved Subcortical and Divergent Cortical Expression of Proteins Encoded by Orthologs of the Autism Risk Gene MET. *Cereb Cortex*, doi:10.1093/cercor/bhq223 (2010).
45 Knoth, R. et al. Murine features of neurogenesis in the human hippocampus across the lifespan from 0 to 100 years. *PLoS One* **5**, e8809, doi:10.1371/journal.pone.0008809 (2010).
46 Mrzljak, L., Uylings, H., Kostović, I. & van Eden, C. Prenatal development of neurons in the human prefrontal cortex. II. A quantitative Golgi study. *J Comp Neurol* **316**, 485-496 (1992).
47 Petanjek, Z., Judas, M., Kostović, I. & Uylings, H. Lifespan alterations of basal dendritic trees of pyramidal neurons in the human prefrontal cortex: a layer-specific pattern. *Cereb Cortex* **18**, 915-929 (2008).
48 Huttenlocher, P. R. & Dabholkar, A. S. Regional differences in synaptogenesis in human cerebral cortex. *J Comp Neurol* **387**, 167-178 (1997).
49 Fertuzinhos, S. et al. Selective depletion of molecularly defined cortical interneurons in human holoprosencephaly with severe striatal hypoplasia. *Cereb Cortex* **19**, 2196-2207 (2009).
50 Zhang, Z. & Reynolds, G. A selective decrease in the relative density of parvalbumin-immunoreactive neurons in the hippocampus in schizophrenia. *Schizophr Res* **55**, 1-10 (2002).

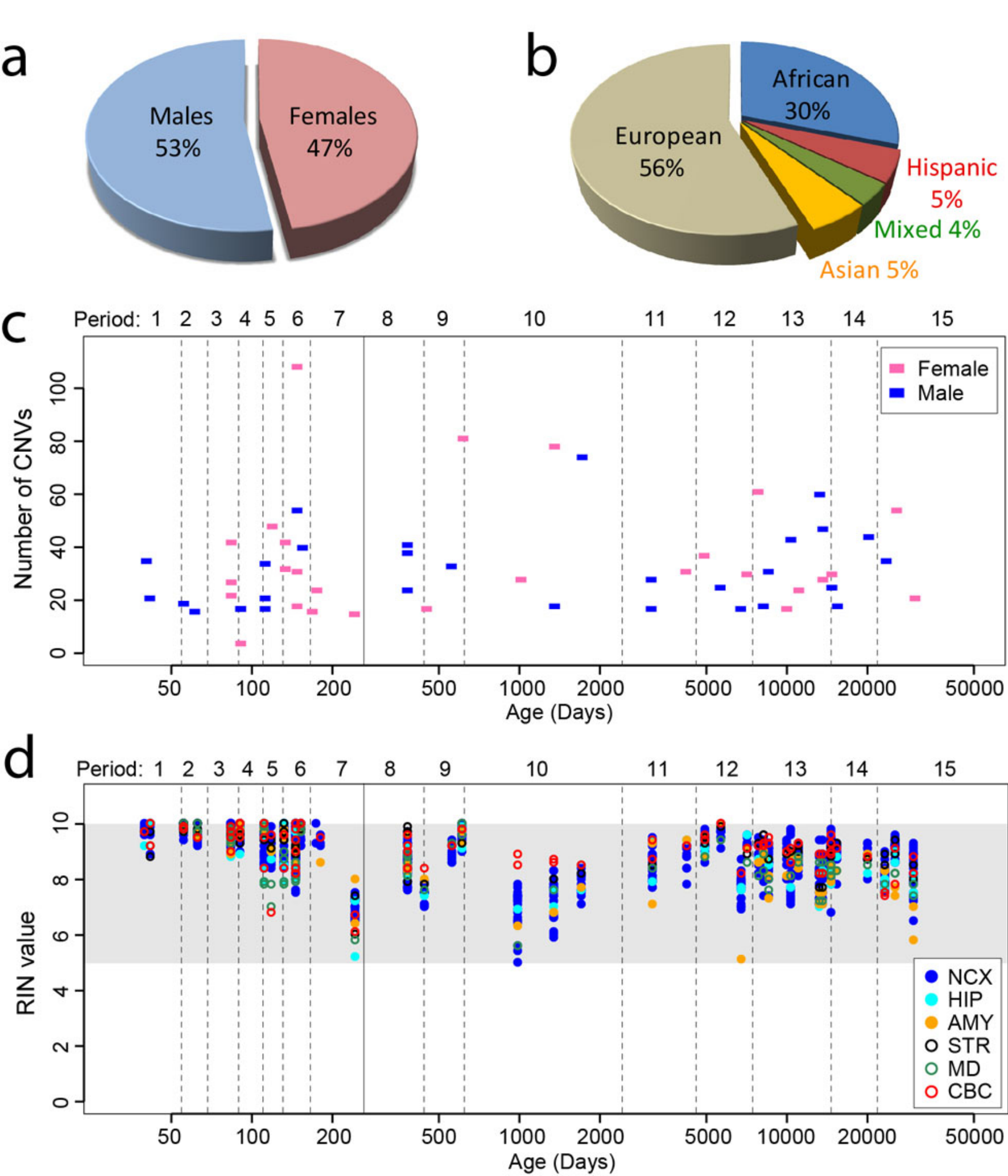
a
Males
53%
Females
47%
b
African
30%
European
56%
Hispanic
5%
Mixed 4%
Asian 5%
c
Period: 1 2 3 4 5 6 7 8 9 10 11 12 13 14 15
Number of CNVs
0 20 40 60 80 100
Female
Male
50 100 200 500 1000 2000 5000 10000 20000 50000
Age (Days)
d
Period: 1 2 3 4 5 6 7 8 9 10 11 12 13 14 15
RIN value
0 2 4 6 8 10
NCX
HIP
AMY
STR
MD
CBC
50 100 200 500 1000 2000 5000 10000 20000 50000
Age (Days)

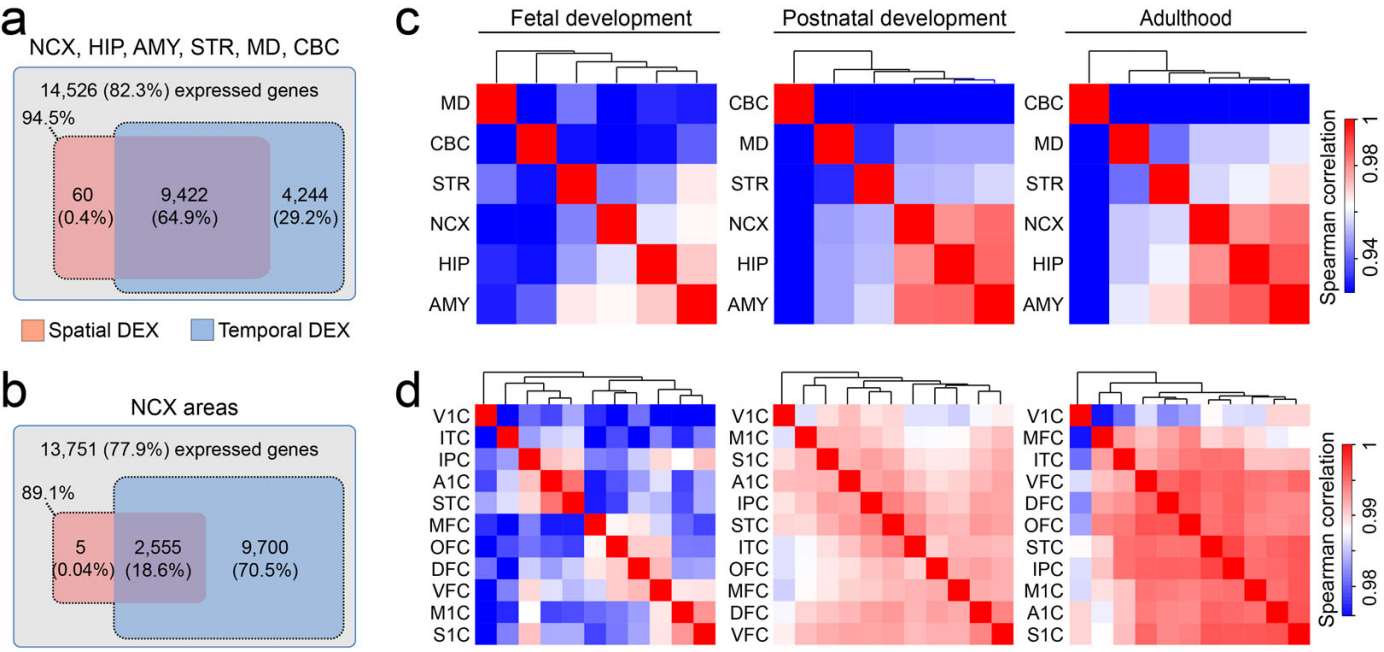
a
NCX, HIP, AMY, STR, MD, CBC
14,526 (82.3%) expressed genes
94.5%
60
(0.4%)
9,422
(64.9%)
4,244
(29.2%)
Spatial DEX
Temporal DEX
b
NCX areas
13,751 (77.9%) expressed genes
89.1%
5
(0.04%)
2,555
(18.6%)
9,700
(70.5%)
c
Fetal development
Postnatal development
Adulthood
MD
CBC
STR
NCX
HIP
AMY
Spearman correlation
1
0.98
0.94
d
V1C
ITC
IPC
A1C
STC
MFC
OFC
DFC
VFC
M1C
S1C
Spearman correlation
1
0.99
0.98

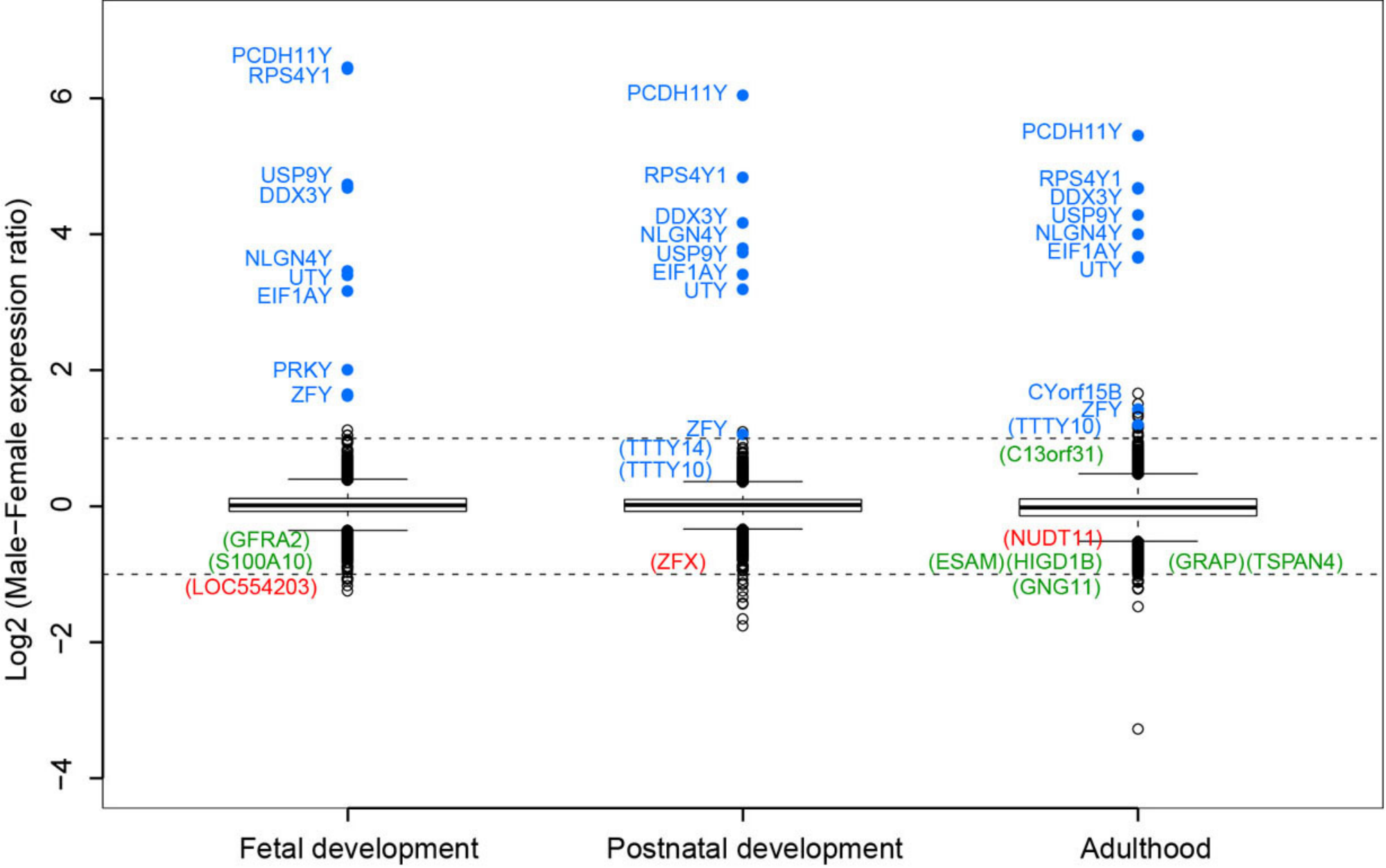
Log2 (Male−Female expression ratio)
6
4
2
0
−2
−4
PCDH11Y
RPS4Y1
USP9Y
DDX3Y
NLGN4Y
UTY
EIF1AY
PRKY
ZFY
(GFRA2)
(S100A10)
(LOC554203)
PCDH11Y
RPS4Y1
DDX3Y
NLGN4Y
USP9Y
EIF1AY
UTY
ZFY
(TTTY14)
(TTTY10)
(ZFX)
PCDH11Y
RPS4Y1
DDX3Y
USP9Y
NLGN4Y
EIF1AY
UTY
CYorf15B
ZFY
(TTTY10)
(C13orf31)
(NUDT11)
(ESAM)(HIGD1B)
(GNG11)
(GRAP)(TSPAN4)
Fetal development
Postnatal development
Adulthood

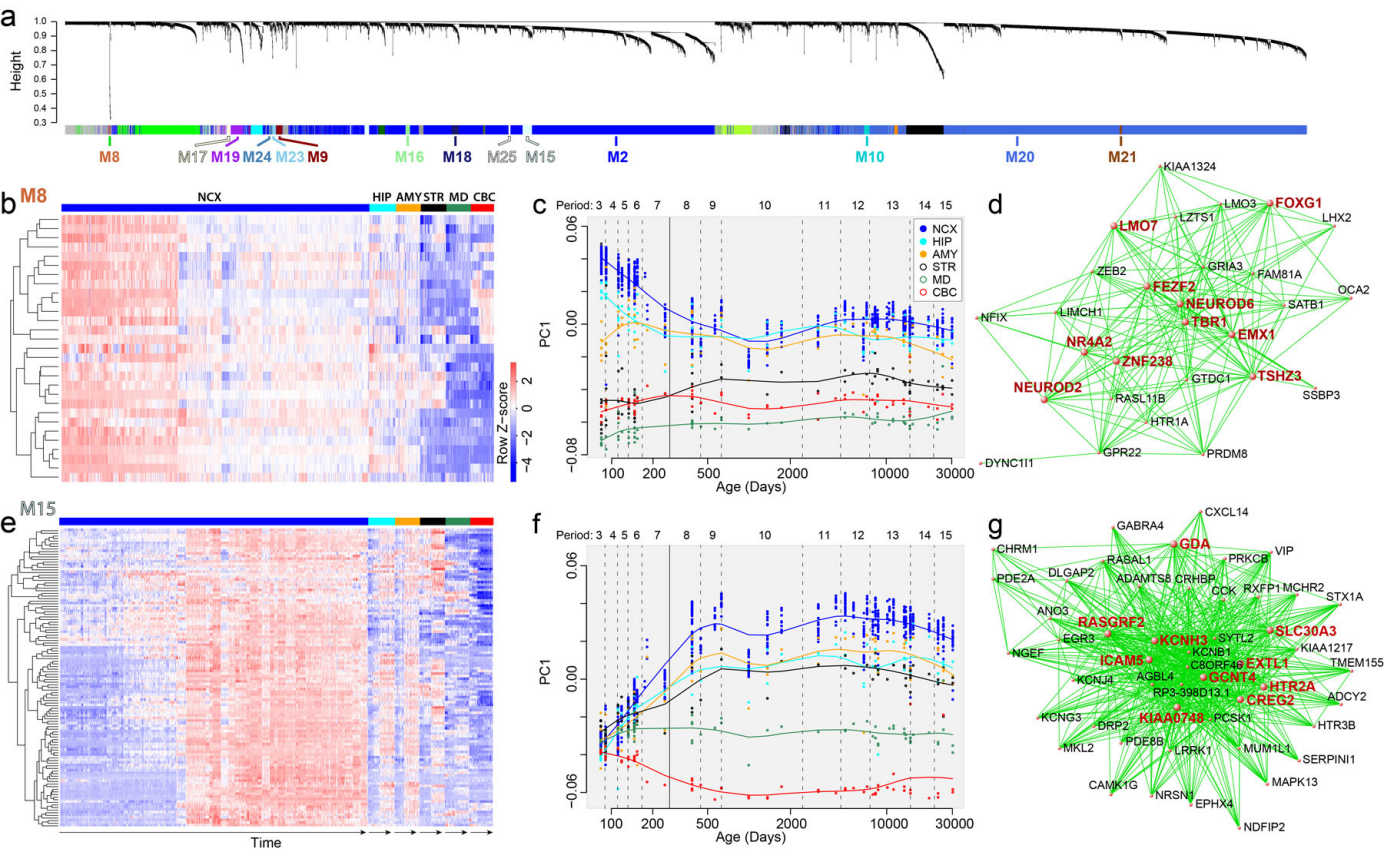
a
Height
1.0
0.9
0.8
0.7
0.6
0.5
0.4
0.3
M8
M17
M19
M24
M23
M9
M16
M18
M25
M15
M2
M10
M20
M21
b
M8
NCX
HIP
AMY
STR
MD
CBC
Row Z-score
c
Period: 3 4 5 6 7 8 9 10 11 12 13 14 15
NCX
HIP
AMY
STR
MD
CBC
PC1
Age (Days)
d
KIAA1324
FOXG1
LMO3
LMO7
LZTS1
LHX2
ZEB2
GRIA3
FAM81A
FEZF2
OCA2
NEUROD6
SATB1
NFIX
LIMCH1
TBR1
EMX1
NR4A2
ZNF238
TSHZ3
NEUROD2
GTDC1
SSBP3
RASL11B
HTR1A
GPR22
PRDM8
DYNC1I1
e
M15
Time
f
Period: 3 4 5 6 7 8 9 10 11 12 13 14 15
PC1
Age (Days)
g
CXCL14
GABRA4
GDA
VIP
CHRM1
RASAL1
PRKCB
PDE2A
DLGAP2
ADAMTS8
CRHBP
CCK
RXFP1
MCHR2
STX1A
ANO3
RASGRF2
SLC30A3
EGR3
KCNH3
SYTL2
KIAA1217
NGEF
KCNB1
C8ORF48
EXTL1
TMEM155
ICAM5
AGBL4
GCNT4
HTR2A
KCNJ4
RP3-398D13.1
CREG2
ADCY2
KCNG3
KIAA0748
PCSK1
HTR3B
DRP2
PDE8B
MKL2
LRRK1
MUM1L1
SERPINI1
CAMK1G
NRSN1
MAPK13
EPHX4
NDFIP2

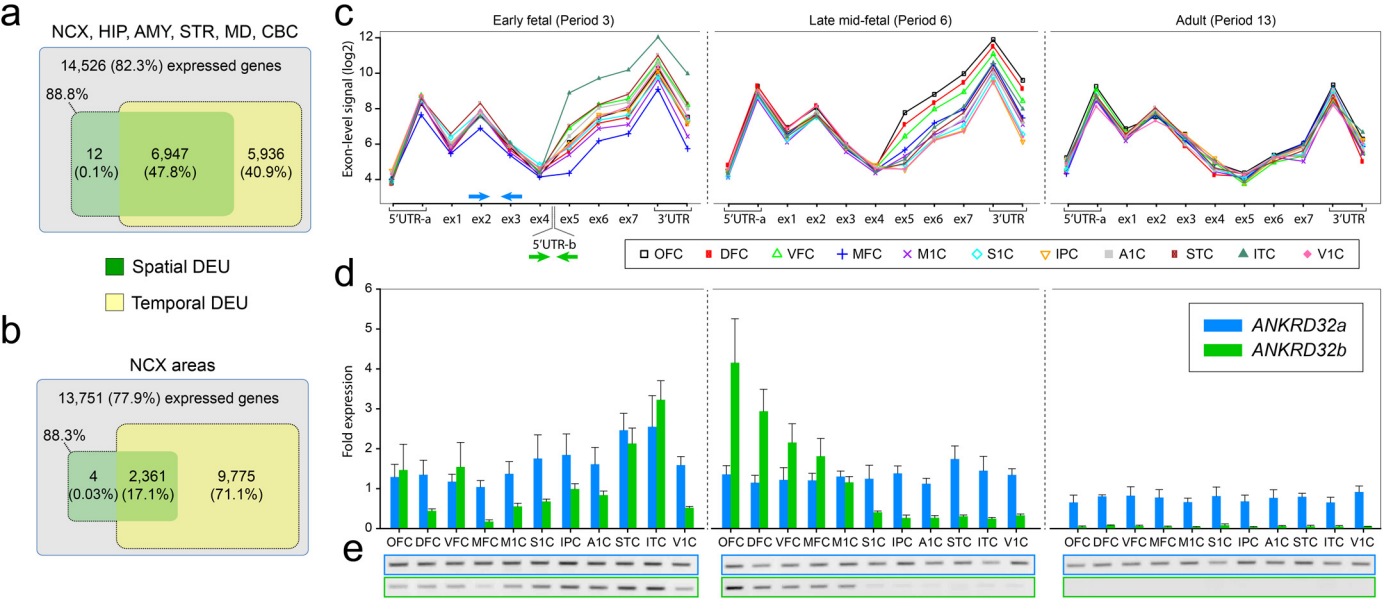
a
NCX, HIP, AMY, STR, MD, CBC
14,526 (82.3%) expressed genes
88.8%
12
(0.1%)
6,947
(47.8%)
5,936
(40.9%)
Spatial DEU
Temporal DEU
b
NCX areas
13,751 (77.9%) expressed genes
88.3%
4
(0.03%)
2,361
(17.1%)
9,775
(71.1%)
c
Early fetal (Period 3)
Late mid-fetal (Period 6)
Adult (Period 13)
Exon-level signal (log2)
5'UTR-a ex1 ex2 ex3 ex4 ex5 ex6 ex7 3'UTR
5'UTR-b
OFC DFC VFC MFC M1C S1C IPC A1C STC ITC V1C
d
Fold expression
ANKRD32a
ANKRD32b
e

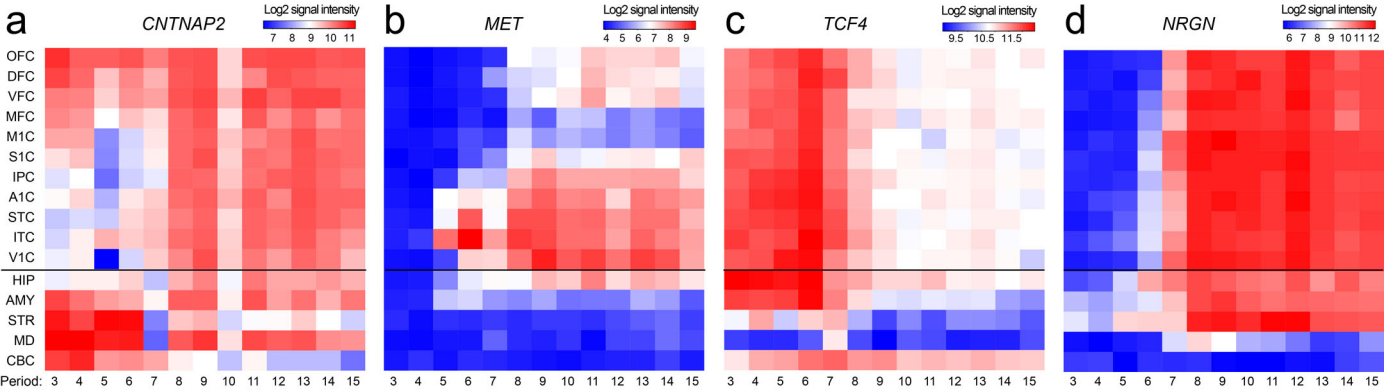
a
CNTNAP2
Log2 signal intensity
7 8 9 10 11
b
MET
Log2 signal intensity
4 5 6 7 8 9
c
TCF4
Log2 signal intensity
9.5 10.5 11.5
d
NRGN
Log2 signal intensity
6 7 8 9 10 11 12
OFC
DFC
VFC
MFC
M1C
S1C
IPC
A1C
STC
ITC
V1C
HIP
AMY
STR
MD
CBC
Period: 3 4 5 6 7 8 9 10 11 12 13 14 15

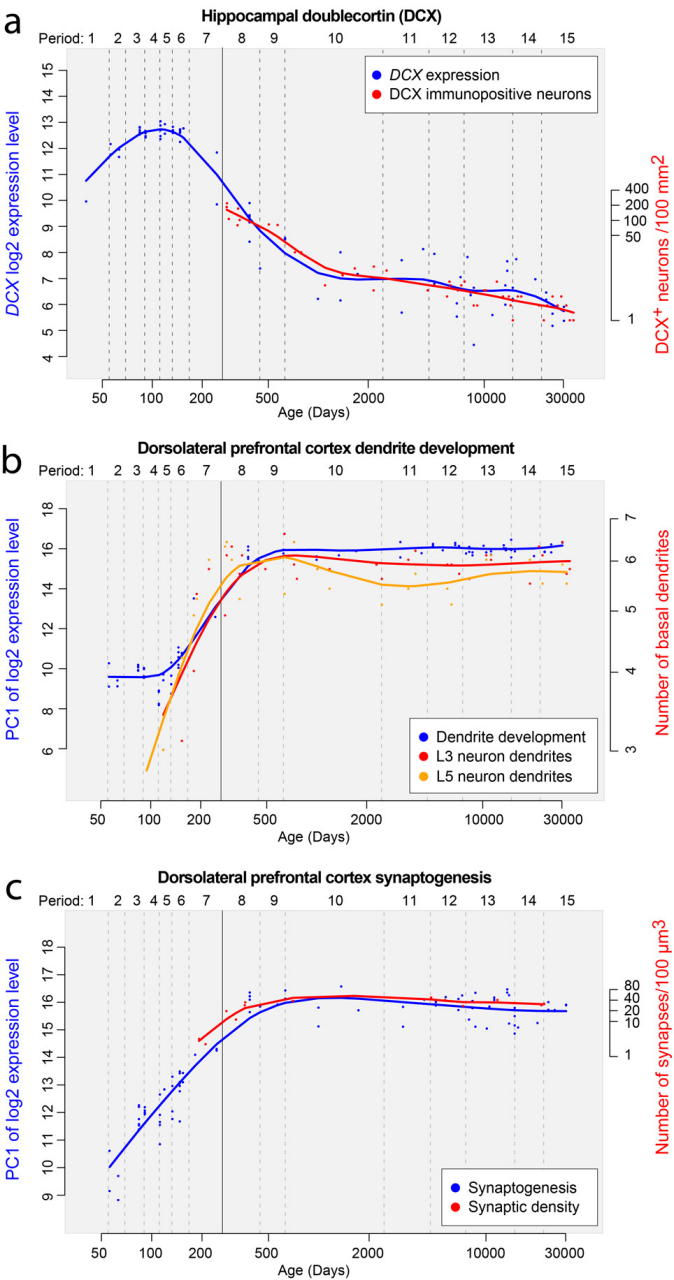
a
Hippocampal doublecortin (DCX)
Period: 1 2 3 4 5 6 7 8 9 10 11 12 13 14 15
DCX log2 expression level
DCX+ neurons /100 mm2
DCX expression
DCX immunopositive neurons
400
200
100
50
1
Age (Days)
50 100 200 500 2000 10000 30000
b
Dorsolateral prefrontal cortex dendrite development
Period: 1 2 3 4 5 6 7 8 9 10 11 12 13 14 15
PC1 of log2 expression level
Number of basal dendrites
Dendrite development
L3 neuron dendrites
L5 neuron dendrites
Age (Days)
50 100 200 500 2000 10000 30000
c
Dorsolateral prefrontal cortex synaptogenesis
Period: 1 2 3 4 5 6 7 8 9 10 11 12 13 14 15
PC1 of log2 expression level
Number of synapses/100 µm3
80
40
20
10
1
Synaptogenesis
Synaptic density
Age (Days)
50 100 200 500 2000 10000 30000

Supplementary Information

Table of Contents

1. Introduction

In this Supplementary Information we provide further information regarding the study design and material and methods. The material and methods sections provide detailed description of the collection, dissection methods, and quality control assessments of post-mortem human brain tissue used in this study. We also provide technical descriptions of data generation and analyses using different platforms. Finally, we present supplementary figures and tables generated from sample metadata and specific gene lists.

2. Supplementary Information on the Study Design

2.1. Definition of periods of human development and adulthood used in this study

We created a classification system of human brain development and adulthood comprised of 15 time periods. Our aim in classifying our samples into different time periods was to be able to broadly compare our data to the majority of published data and to have the precision to allow for detection of transcriptional changes that may occur with high temporal specificity during prenatal and early postnatal periods. To avoid confusion with the well-known Carnegie stages for embryonic human brain[51], we divided our specimens into developmental periods covering both prenatal and postnatal development and adulthood. At the present, well-defined morphological staging is limited to the embryonic development, and no fully satisfactory staging system has yet been devised for the fetal and early postnatal development. In this study, we have specified time periods based mainly on the timing and progression of major neurodevelopmental events in the cerebral cortex, a structure that is central to the highest cognitive functions in humans and is arguably one of the most studied human brain structures. Our system took into consideration previous developmental classifications of the human brain[51-56]. Human brain development can be broadly divided into two periods: prenatal and postnatal. Although prenatal development is relatively short in comparison to postnatal development, it is highly dynamic. Thus we divided prenatal development into seven distinct periods to facilitate high temporal resolution. For postnatal developmental periods we considered cognitive, motor, social, and emotional milestones outlined by the Department of Human Health and Services (http://www.cdc.gov/ncbddd/child/). As pointed out by leading experts[51] prenatal age is postfertilizational by definition, thus for prenatal age we used postconceptional weeks (PCW) to include both proper terms used in current literature: postfertilizational (timed from the fertilization of the ovum) and postovulatory (timed from the ovulation). Although there is a small difference in the timing of these events, these three terms (postconceptional, postfertilizational and postovulatory) can be used as synonyms.. The following is a brief description of the periods as defined in this study.

Period 1 (Embryonic development, 4≤ Age <8 PCW) corresponds to late embryonic development defined by the first lamination of the cerebral wall (i.e., ventricular zone, subventricular zone, intermediate zone, marginal zone). Early embryonic processes (e.g., formation of the neural tube, closure of the neuropores, formation of the primary and secondary brain vesicles) are completed in this period. This period is marked by extensive proliferation and the initiation of neurogenesis. The first axons invade the cerebral wall during this period as well.

Period 2 (Early fetal development, 8≤ Age <10 PCW) is characterized by the appearance and subsequent primary consolidation of the cortical plate. Deep layer neurons are generated and begin radially migrating to their proper position in the cortical plate. The secondary proliferative zone, the subventricular zone, appears around 8 PCW. The internal capsule and anterior commissure begin to appear. Major neuroanatomical fetal landmarks are readily recognized during this period, including the ventricular zone, subventricular zone, intermediate zone, presubplate zone (i.e., precursor of future subplate proper), cortical plate, marginal zone, and subpial granular layer can be distinguished in the cerebral wall.

Period 3 (Early fetal development, 10≤ Age <13 PCW) is characterized by the presence of the bilaminate cortical plate. Namely, the deep part of the cortical plate itself becomes delaminated and together with a thin, cell-sparse band of tissue (described as the presubplate in a previous period) represents the subplate in formation. The first synapses are formed in the marginal zone above the cortical plate and in the presubplate zone below the cortical plate, whereas the cortical plate remains free of synapses. Tangential migration of GABAergic interneurons can be observed. Proliferation and migration of neurons are the two main histogenetic processes that occur during this period. The corpus callosum can be identified during this period. Afferent projections start to invade the cortical anlage and are primarily monoaminergic. The first sulci start to appear in this period (i.e., lateral and callosal sulcus).

Period 4 (Early mid-fetal development, 13≤ Age <16 PCW) is characterized by the secondary consolidation of the cortical plate concomitantly with the formation of a large, synapse-rich subplate zone. The first cortical neurons show signs of morphological differentiation. After its formation and during subsequent mid-fetal periods, the subplate zone serves as a waiting compartment for afferent axons from several subcortical structures. Proliferation and migration of neurons and ingrowth of afferent axons are the major histogenetic events occurring during this period. At this period and subsequent prenatal periods, typical fetal lamination pattern of the cerebral wall can be observed. The cerebral wall can be divided into six major architectonic compartments or fetal zones: ventricular zone, subventricular zone, intermediate zone, subplate zone, cortical plate, and marginal zone, which contains a transient subpial granular layer.

Period 5 (Early mid-fetal development, 16≤ Age <19 PCW) is characterized by an increase in the size of the subplate zone and the overall thickness of the cerebral wall. Ingrowth of thalamocortical axons into the subplate and migration of upper cortical layer projection neurons are major histogenetic events. The parieto-occipital, cingulate, and calcarine sulci appear in this period.

Period 6 (Late mid-fetal development, 19≤ Age <24 PCW) is characterized by the peak of subplate zone thickness and development, and by the massive ingrowth of afferent axons from the subplate zone into the cortical plate. Therefore, the first synapses can be observed in the neocortical plate. Neurogenesis ceases in the pallial wall but still continues in the subpallial ganglionic eminences during this period. The central sulcus, superior temporal sulcus, collateral sulcus, superior temporal gyrus, and parahippocampal gyrus can be identified.

Period 7 (Late fetal development, 24≤ Age <38 PCW) is characterized by the transformation of the typical fetal lamination pattern into an adult-like lamination pattern of the cerebral wall. Resolution of the subplate zone starts and the Brodmann's "six-layered ontogenetic Grundtypus" (i.e., the fetal equivalent of future layers 2–6) appears within the cortical plate during this period. Cytoarchitectonic regional and areal differentiation of the cortical plate/cortex is an important event that occurs during this period. Neuronal differentiation, ingrowth of thalamocortical axons, and gliogenesis are major histogenetic processes observed during this period. Synaptogenesis continues primarily in the cortex. Myelination of select cortical axon projections starts in this period. The ventricular zone gradually thins until it appears as a single layer of cuboidal/columnar cells. Majority of cortical gyri and sulci appear during this period.

Period 8 (Neonatal and early infancy, birth ≤ Age <6 postnatal months) is characterized by reorganization of long afferent and corticocortical axons, transformation and maturation of cortical layers (especially layer 6 and 5) from the fetal to an adult-like pattern, and rapid synaptogenesis and spinogenesis. The remnants of the subplate zone, although resolving, are still present below layer 6 and thus form a transition from immature cortex to the developing gyral white matter. Specific motor (e.g., grasping, raising of the head, stretching of the legs and kicking) and sensory (e.g., object following, head turning toward sound) skills appear during this period.

Period 9 (Late infancy, 6≤ Age <12 postnatal months) is characterized by further development of motor skills (e.g., sitting with and without support), sensory skills (e.g., development of color vision), and cognitive skills (e.g., exploration with hand and mouth, response to one's own name). Resolution of the subplate zone is completed and neurons that survive resolution of the subplate zone are incorporated into the subcortical (gyral) white matter as interstitial neurons.

Period 10 (Early childhood, 1≤ Age <6 years) is characterized mainly by reorganization and maturation of local circuits, and the peak of synaptogenesis. During this period rapid development of motor skills (e.g., walking, pincer grasp, fine movement control), social and emotional skills (e.g., development of imitation, self-awareness, independence), and cognitive skills (e.g., thinking, mathematical abilities, language) is observed.

Period 11 (Middle and late childhood, 6≤ Age <12 years) is characterized by further cognitive development and refinement of neural circuits.

Period 12 (Adolescence, 12≤ Age <20 years) is characterized by sexual maturation and the appearance of adult-like connectivity pattern.

Period 13 (Young adulthood, 20≤ Age <40 years) is characterized by the end of maturation processes in the brain (e.g., myelination ends in the first part of this period) and appearance of an adult-pattern of brain functions.

Period 14 (Middle adulthood, 40≤ Age <60 years) is characterized by an adult-like pattern of brain functions and the beginning of aging processes.

Period 15 (Late adulthood, 60 years +) is characterized by the progression of aging processes.

2.2. Ontology and anatomical definition of sampled brain regions and NCX areas

Brain development is a highly dynamic process during which each region undergoes distinct organizational and maturational changes. Thus, we created a structural ontology that contains brain structures (e.g., NCX areas, HIP, AMY, STR, MD, CBC) that are well defined throughout most of time periods, and several transient structures (e.g., MGE, LGE, CGE, URL). In total, 8 structures were analyzed for period 1, 10 regions for period 2, and up to 16 regions for periods 3 – 15. Below we describe this ontology and anatomical definition of sampled brain regions and NCX areas based on histological verification.

2.2.1. Neocortex (NCX)

Samples collected from period 1 and 2 specimens contained the entire thickness of the cerebral wall. Samples collected from period 3–7 specimens contained the marginal zone, cortical plate, and part of the underlying subplate (Supplementary Fig. 3). Samples from period 8–15 specimens were dissected such that the entire gray matter (layer 1-6) and part of the underlying subplate (periods 8 and 9) or white matter (periods 10 – 15) were collected (Supplementary Fig. 3). Nissl staining of the neighbouring thin block was used to histologically verify the identity of the dissected area and to microscopically evaluate tissue. Neocortical cytoarchitecture of each sample was compared to areal cytoarchitectonic maps to distinguish Brodmann areas (BA)[57]. Samples with incorrect cytoarchitecture or abnormal microscopical appearance were excluded from the study. Neocortical areas (see below) were grouped according to the lobes from which they were sampled.

2.2.1.1. Frontal cortex (FC)

For ***period 1***, the sampled area corresponded to the anterior third of telencephalic vesicle (cerebral wall) corresponding to prospective FC.

For ***period 2***, the sampled area corresponded to different parts (orbital (OFC), dorsolateral (DFC), ventrolateral (VFC), and medial (MFC) of the anterior part of telencephalic vesicle (cerebral wall) corresponding to prospective FC. In addition, paracentral region corresponding approximately to the prospective motor and parietal somatosensory (M1C/S1C) cerebral wall was dissected as one sample (MSC).

For ***periods 3 – 7***, prior to the appearance of all gyri and sulci, multiple areas of the FC were sampled as follows (Supplementary Fig. 2):

- **Orbital prefrontal cortex (OFC)** was sampled from the middle part of the orbital surface of the cerebral hemisphere, immediately next to the prospective gyrus rectus.
- **Dorsolateral prefrontal cortex (DFC)** was sampled from the middle third of the dorsolateral surface of anterior third of the cerebral hemisphere.
- **Ventrolateral prefrontal cortex (VFC)** was sampled from the posterior part of the frontal operculum, above the lateral sulcus and prospective insula.
- **Medial prefrontal cortex (MFC)** was sampled from the perigenual and subgenual region of the medial surface.
- **Primary motor cortex (M1C)**, prior to the appearance of the central sulcus, was sampled from the anterior third of the middle third of the cerebral hemisphere, medial third and upper part of the lower third of the dorsolateral surface. We used the striatum at the septal level as the landmark between the anterior and middle one third of the dorsolateral cortical surface. In some cases, we sampled M1C and S1C areas as single area and termed it motor-somatosensory cortex (**M1C/S1C**) due to the lack of clear anatomical and histological boundaries between immature M1C and S1C. After the appearance of the central sulcus M1C was sampled in front of the central sulcus from the middle and upper part of the lower third of the dorsolateral surface of the hemisphere.

For ***periods 8–15***, sampled areas were as follows (Supplementary Fig. 1):

- OFC was sampled from the anterolateral two thirds of the orbital gyri. OFC corresponds approximately to BA 11.
- DFC was sampled from approximate border between the anterior and middle third of the medial frontal gyrus. DFC corresponds approximately to BA 9 and 46.
- VFC was sampled from the posterior third of the inferior frontal gyrus, corresponding to the opercular and triangular part of the inferior frontal gyrus. VFC corresponds approximately to BA 44 and 45.
- MFC was sampled from perigenual and subgenual parts of the anterior cingulate gyrus and the anteromedial part of the superior frontal gyrus. MFC corresponds approximately to BA 24, 32 and 33.
- M1C was sampled from the ventrolateral part of the precentral gyrus, corresponding most closely to the orofacial region of M1C. M1C corresponds to BA4.

2.2.1.2. Parietal cortex (PC)

For ***period 1***, the sampled areas corresponded to the dorsal middle third of the cerebral wall.

For ***period 2***, the sampled areas included the paracentral region corresponding approximately to the prospective motor and parietal somatosensory (M1C/S1C) cerebral wall, and the posterior half of the dorsal middle third of the cerebral wall corresponding approximately to the prospective inferior parietal cortex (IPC).

For ***periods 3 – 7***, prior to the appearance of gyri and sulci, multiple areas of the PC were sampled as follows (Supplementary Fig. 2):

- **Primary somatosensory cortex (S1C)**, prior to the appearance of the central sulcus, was sampled immediately caudal to the M1C (see M1C description above). After the appearance of the central sulcus,

S1C was sampled behind the central sulcus from the middle and upper part of the lower third of the dorsolateral surface of the cerebral hemisphere adjacent to the M1C area.

- **Posterior inferior parietal cortex (IPC)** was sampled from the lower posterior part of the dorsolateral surface of the middle third of the cerebral hemisphere adjacent to the end of the lateral sulcus.

For ***periods 8–15***, sampled areas were as follows (Supplementary Fig. 1):

- S1C was sampled from the ventrolateral part of the postcentral gyrus adjacent to the M1C area. S1C corresponds to BA 1–3.
- IPC was sampled from the posterior half of the supramarginal gyrus. IPC corresponds approximately to BA 40.

2.2.1.3. Temporal cortex (TC)

For ***period 1***, the sampled area corresponded to the anterior two thirds of the lateral part of the posterior third of the cerebral wall.

For ***period 2***, the sampled areas included the posterior two thirds of TC corresponding approximately to the prospective auditory and superior temporal cortex (A1C/STC) cerebral wall, and the anterior third corresponding approximately to the prospective inferior temporal cortex (ITC).

For ***periods 3 – 7***, prior to the appearance of gyri and sulci, multiple areas of the TC were sampled as follows (Supplementary Fig. 2):

- **Primary auditory cortex (A1C)** was sampled from the upper part of the temporal bank of the lateral sulcus.
- **Posterior superior temporal cortex (STC)** was sampled from the upper part of the superior third of the temporal lobe adjacent to the lateral sulcus and A1C area.
- **Inferior temporal cortex (ITC)** was sampled from the lower part of the inferior third of the temporal lobe adjacent to the temporal lobe pole.

For ***periods 8–15***, sampled areas were as follows (Supplementary Fig. 1):

- A1C was sampled from the planum temporale and the transverse temporal gyri. A1C corresponds to BA 41.
- STC was sampled from the posterior third of the superior temporal gyrus. STC corresponds approximately to BA 22.
- ITC was sampled from the anterior third of the inferior temporal gyrus. ITC corresponds approximately to BA 20.

2.2.1.4. Occipital cortex (OC)

For ***periods 1 and 2***, sampled tissue corresponded to the posterior (occipital) part of the cerebral wall.

For ***periods 3 – 7***, (Supplementary Fig. 2) prior to the appearance of gyri and sulci, sampled tissue corresponded to prospective **primary visual cortex** (**V1C**). Prior to the appearance of the calcarine fissure, V1C was sampled from the posterior third of the medial wall of the prospective occipital lobe. After appearance of the calcarine fissure, V1C was sampled as described below.

For ***periods 8–15***, (Supplementary Fig. 1) V1C was sampled from the area surrounding the calcarine fissure. Only samples in which the stria of Gennari could be recognized were included. V1C corresponds to BA 17. Small pieces of the neighbouring BA18 could have been occasionally present in the sample, but the majority of the sample corresponded to BA17.

2.2.2. Hippocampus (**HIP**)
For ***periods 1 and 2***, HIP was sampled from the hippocampal anlage, located on the ventromedial side of the cerebral hemisphere.

For ***periods 3–15***, (Supplementary Figs. 1 and 2) HIP was sampled from the middle third of the retrocommissural hippocampal formation, located on the medial side of the temporal lobe. Sampled areas always contained dentate gyrus and the cornu ammonis.

2.2.3. Amygdala (AMY)
We aimed at dissecting the whole AMY from ***periods 3–15*** specimens (Supplementary Figs. 1 and 2). Very small quantities of surrounding white matter and potentially other surrounding structures in the basal telencephalon were included in samples.

2.2.4. Ventral forebrain (VF)
Depending on the time period we sampled different parts of the VF. For ***period 1***, the sampled region corresponded to the ventral forebrain (VF), which included primordium of the ganglionic eminence.

2.2.4.1. Medial ganglionic eminence (MGE)
2.2.4.2. Lateral ganglionic eminence (LGE)
2.2.4.3. Caudal ganglionic eminence (CGE)
We sampled the MGE, LGE and CGE separately from ***period 2*** specimens.

2.2.4.4. Striatum (STR)
Striatum (**STR**) was sampled from ***periods 3–15*** specimens (Supplementary Figs. 1 and 2). We dissected the anterior part of striatum containing the head of the caudate nucleus and the putamen, separated by the internal capsule and ventrally connected to the nucleus accumbens.

2.2.5. Diencephalon (DIE)
Depending on the time period we sampled different parts of the DIE. For ***period 1***, the sampled region corresponded to the entire DIE.

2.2.5.1. Dorsal thalamus (DTH)
For ***period 2***, the sampled region corresponds to the dorsal part of the thalamic anlage (**DTH**).

2.2.5.2. Mediodorsal nucleus of the thalamus (MD)
For ***periods 3–15*** (Supplementary Figs. 1 and 2), the whole mediodorsal nucleus of the thalamus (**MD**) was sampled from the dorsal and medial thalamus. Small quantities of surrounding thalamic tissue could be present in the samples.

2.2.6. Upper (rostral) rhombic lip (URL)
Sampled region corresponds to the **URL** and adjacent tissue located above the upper rhomboid fossa for ***periods 1 and 2***.

2.2.6.1. Cerebellar cortex (CBC)
CBC was sampled from the lateral part of the posterior lobe for ***periods 3–15*** (Supplementary Figs. 1 and 2). The sampled area contained all three layers of cerebellar cortex and underlying white matter but not the deep cerebellar nuclei. CBC approximately corresponds to the lateral pontocerebellum.

3. Tissue Samples

3.1. Tissue procurement

This study was conducted using postmortem human brain specimens from tissue collections at the Department of Neurobiology at Yale University School of Medicine and the Clinical Brain Disorders Branch of the National Institute of Mental Health. Additional specimens were procured from the Human Fetal Tissue Repository at the Albert Einstein College of Medicine (AECOM), the Brain and Tissue Bank for Developmental Disorders at the University of Maryland, the Birth Defects Research Laboratory at the University of Washington, Advanced Bioscience Resources Inc. and the MRC-Wellcome Trust Human Developmental Biology Resource at the Institute of Human Genetics, University of Newcastle, UK. Tissue was collected after obtaining parental or next of kin consent and with approval by the institutional review boards at the Yale University School of Medicine, the National Institutes of Health, and at each institution from which tissue specimens were obtained. Tissue was handled in accordance with ethical guidelines and regulations for the research use of human brain tissue set forth by the NIH (http://bioethics.od.nih.gov/humantissue.html) and the WMA Declaration of Helsinki (http://www.wma.net/en/30publications/10policies/b3/index.html).

Appropriate written informed consent was obtained and all available non-identifying information was recorded for each specimen. Specimens range in age from 5.7 post-conceptual weeks (PCW) to over 80 years. Of 57 post-mortem brain specimens included in this study, 24 were obtained with either left or right hemisphere, and 33 were obtained with both hemispheres. Embryonic and fetal age was extrapolated based on the date of the mother's last menstruation, characteristics of the fetus noted upon ultrasonographic scanning, foot length of the fetus, and visual inspection. The post-mortem interval (PMI) was defined as hours between time of death and time when tissue samples were frozen.

3.2. Neuropathological evaluation

All clinical histories, tissue specimens, and histological sections were evaluated to assess for hypoxia, cerebrovascular incidents, tumours, microbial infections, neurodegeneration, demyelination, and metabolic disease. In addition, cadavers from period 4 onward underwent a complete autopsy and were refrigerated beforehand to minimize degradation. To prepare tissue sections for microscopic neuropathalogical histological examination, small samples (usually the dorsal parietal cortex, striatum with ependymal layer and subependymal zone, hippocampus, and cerebellar cortex) of fresh or frozen tissue were dissected and fixed in 4% paraformaldehyde and processed for immunohistochemistry as described below.

3.3. Selection criteria for brain specimens

To better ensure consistency between samples and decrease potential variation due to ante- and post-mortem conditions, specific selection criteria were arbitrarily established. Most postnatal and adult brains also underwent comprehensive toxicological screening. The aim was to collect tissue specimens from clinically unremarkable donors without history or signs of neurological or neuropsychiatric illness or drug abuse. The following selection criteria were strictly adhered to when deciding whether to exclude or include each brain specimen.

- Brains with chromosomal or large-scale genomic abnormalities, detected by karyogram and/or Illumina Human Omni-2.5, were excluded.
- Prenatal and neonatal specimens were excluded if drug or alcohol abuse by the mother during pregnancy was reported or if potassium chloride, salt water, or urea were injected into the amniotic sac during surgical procedure.
- Only brains free of obvious malformations or lesions were collected. Disqualifying characteristics included any obvious abnormality of the neural tube, forebrain, brainstem, cranial nerves, cerebellum, or spinal cord (i.e., prominent intraparenchymal haemorrhage and ischemia, infection, periventricular leukomalacia, abnormal meninges, dysplasia, hypoplasia, alterations in the pial or ventricular surface, extensive white matter lesions).

- Samples were excluded if microscopic analysis revealed extensive neuronal loss, neuronal swelling, glioneuronal heterotopias, or dysmorphic neurons and neurites.
- Samples that tested positive for Hepatitis B, Hepatitis C, or HIV were excluded.
- Early postnatal and adult (periods 8–15) specimens were excluded if excessive drug or alcohol abuse was reported, if the individual had any known neurological or psychiatric disorders, or if any prolonged agonal conditions (coma, prolonged pyrexia, hypoxia, seizures, prolonged dehydration, hypoglycaemia, multiple organ failure) were reported. Other excluding factors included ingestion of neurotoxic substances at the time of death, suicide, severe head injury, significant haemorrhages, widespread vascular abnormalities, ischemia, tumours, stroke, congenital neural abnormalities, and signs of neurodegeneration (spongiosis, amyloid plaques, Lewy bodies, and amyloid angiopathy).

3.4. Tissue processing and dissections

Depending on the condition and period of the procured specimens, four different dissection methods were used. All dissections were video documented using a Canon PowerShot A470 digital camera (periods 1 and 2) or a Sony HDR-CX150 HD-camera (periods 3–15). Regions of interest were matched between different specimens, ages, and hemispheres of each brain. Supplementary Table 3 provides a complete list of all tissue samples for which we have included Exon array data in this study. Specific dissection protocol depended upon the period of the specimen and the method by which it was preserved. For all brain specimens procured at Yale University School of Medicine and the Human Fetal Tissue Repository at AECOM, brain regions and NCX areas of interest (Supplementary Table 1) were collected from fresh tissue. For all other specimens, regions/areas were collected from frozen tissue slabs or whole specimens stored at -80 ºC. To ensure consistency between specimens, all dissections were performed by the same person (N. S.). Small samples of fresh or frozen cerebellar cortex were used to measure tissue pH.

3.4.1. Tissue dissection methods

Different dissection procedures were used for each specimen, depending upon the period of the brain (see below). Our pilot experiments indicated that the quality of RNA and DNA was largely unaffected by variation between the dissection methods used.

3.4.1.1. Regional sampling from fresh brain specimens

Brains were chilled on ice for 15–30 minutes prior to sectioning. Brains were placed ventral side up onto a chilled aluminium plate (1 cm thick) on ice. The brainstem and cerebellum were removed from the cerebrum by making a transverse cut at the junction between the diencephalon and midbrain. Next, the cerebrum was divided into left and right hemispheres by cutting along the midline using a Tissue-Tek Accu-Edge trimming blade, 260 mm. The cerebellum was separated from the brainstem by cutting directly posterior to the brainstem, along the cerebellar peduncles. The regions of interest were dissected using a scalpel blade and immediately frozen in liquid nitrogen. Dissected samples were either immediately processed for RNA extraction or stored at -80 °C for later RNA extraction. The remaining brain tissue was cut to obtain 1 cm (periods 5–15 specimens) or 0.5 cm (periods 3 and 4 specimens) thick serial, coronal sections. The tissue slabs were snap frozen in isopentane/dry ice at -30 to -40 ºC and stored at -80 ºC.

3.4.1.2. Regional sampling from frozen brain specimens

All previously frozen periods 3–15 specimens and tissue slabs were microscopically inspected and the desired region was demarcated, then dissected using a dental drill (AnyXing, 300D) and a Lindemann Bone Cutter H162A.11.016 or diamond disk saw (Dental Burs USA; r=11 mm) on a 1 cm thick aluminium plate over dry ice. Dissected tissue samples were stored at -80 ºC prior to further processing.

3.4.1.3. Regional sampling from specimens processed in RNA*later*

Frozen period 2 specimens were sectioned coronally at approximately 2 mm, beginning at the frontal pole, using a dental diamond disk saw. For gradual thawing, tissue slabs were transferred from -80 °C

storage to overnight storage in RNA*later* ICE (Ambion) at -20 °C. Tissue slabs were visually inspected for gross anatomical neuropathological abnormalities. Next, regions of interest were sampled under a dissection microscope at 4 °C, and stored in Buffer RLT Plus from the RNeasy Plus Mini Kit (Qiagen) at 4 °C. RNA was immediately extracted.

3.4.2. Histological verification of tissue sampling

To verify that the region or NCX area of interest is properly and consistently sampled, we also collected small tissue blocks, from both frozen and fresh brain specimens, adjacent to the tissue sample dissected for the RNA extraction. We have done this for the majority of M1C, S1C, IPC, A1C and V1C samples, which in our experience were hard to match across different specimens but can be histologically verified using Nissl method in postnatal specimens due to cytoarchitectonic differences. This method was also occasionally used for other regions or NCX areas. These tissue blocks were then fixed in 4% paraformaldehyde for 48 h, sectioned at 50 µm thickness using a vibratome, and Nissl stained to verify the identities of dissected adjacent tissue (examples of Nissl stained brain regions and NCX areas from a fetal and adult brain are provided in Supplementary Fig. 4).

3.4.3. Dissection scoring

We developed a scoring system to evaluate the precision of how well the sampled region/area was represented at the same position of corresponding samples of the same period.

Score	Sample description
1 or **2**	The region/area of interest was absent (1) or largely absent (2) and thus not collected.
3	The region/area of interest was not complete but was of suitable quality to collect.
4	The region/area of interest was largely intact but was not histologically verified or could not be collected at precisely the same position from which the corresponding contralateral sample was collected.
5	The region/area of interest was fully intact, verified by gross inspection or Nissl staining (NCX areas), and collected at precisely the same position as corresponding samples of the same period.

3.4.4. Tissue pulverization. To ensure proper representation of the region of interest, frozen tissue samples were pulverized in liquid nitrogen using a ceramic mortar and pestle (Fisher Scientific, cat# 12-961C and 12-961-5C). Pulverized samples were transferred to wide-mouth cryogenic vials (Nalgene, cat# 03-337-7B) and stored at -80 ºC until used for RNA extraction.

4. DNA and RNA processing and analysis

4.1. DNA extraction and genotyping

For genotyping analysis, up to 25 mg of brain tissue, usually collected from the CBC, was homogenized using a bead mill homogenizer (Bullet Blender, Next Advance) and lysed in Buffer ATL (Qiagen) at 56 °C for 3–4 hrs. Genomic DNA was isolated using a non-phenolic procedure (DNeasy Blood & Tissue Kit, Qiagen) followed by proteinase K and RNase A treatment (Qiagen). Optical density values of extracted DNA were measured using a NanoDrop (Thermo Scientific) and PicoGreen dsDNA assay kit (Invitrogen). DNA integrity was confirmed by agarose gel electrophoresis. Illumina Omni-2.5 million SNP arrays were used for

genotyping. DNA samples were processed according to the Infinium HD Assay Super, Automated Protocol for Human Omni 2.5-Quad Bead Chip (Illumina).

4.2. Copy number variation (CNV) analysis and genomic quality control

All SNP chips were scanned using the Illumina iScan system. The intensity files were analyzed using Illumina GenomeStudio v2010.2 software. Gender of each sample was determined from the SNP genotyping results using GenomeStudio to confirm the metadata of each sample. Two algorithms were used to detect CNV from SNP intensity data. The cnvPartition algorithm in GenomeStudio was used to detect CNV. The measurement of B allele frequency and log-transformed R ratio of all SNPs were exported to the program PennCNV to confirm CNVs. The two sets of results were compared and only CNVs detected by both algorithms were included in the final results. Only specimens (N=57) with no signs of chromosomal or large-scale genomic abnormalities were included in the study.

4.3. Corroborating and refining ethnic background from genotypes

Ethnicity of donors was reported by next of kin. However, in the majority of prenatal and some postnatal cases the ethinicity of the father was not available. For this reason, the ethnic background was corroborated and refined by comparing SNP analysis of each individual to SNP data available in HapMap III. The whole allele frequency data set of the following ethnic populations was downloaded from HapMap III (ftp://ftp.ncbi.nlm.nih.gov/hapmap/frequencies/2010-08_phaseII+III/): (1) Utah residents of Eastern and Western European descent (CEU); (2) Toscani in Italy (TSI); (3) Yoruba, in Ibadan, Nigeria (YRI); (4) African ancestry in Southwest USA (ASW); (5) Luhya in Webuye, Kenya (LWK); (6) Maasai in Kinyawa, Kenya (MKK); (7) Chinese in Metropolitan Denver, Colorado (CHD); (8) Japanese in Tokyo, Japan (JPT); (9) Mexican ancestry in Los Angeles, California (MEX) and (10) Gujarati Indians in Houston, Texas (GIH).

A group of SNPs frequently expressed in some populations but rarely in others was first selected. The maximum allele frequency and minimum allele frequency in the 10 populations were calculated for each SNP. Population specific SNPs were defined as those for which the difference between the maximum and minimum allele frequency was greater than 0.6. These population-specific SNPs were cross-referenced against the SNPs identified by genotyping of our samples. Only the common set of SNPs was used in the following calculation.

The common set of SNPs is designated as S_i, where i is a variable value that represents a specific SNP. The genotype G_i of SNP S_i could be AA, AB or BB, where A and B are two alleles for the SNP. The populations are designated as P_j, where j is a value of 1 through 10 that represents a specific ethnicity, as defined above. The A-allele frequency of SNP S_i within population P_j is f_{ij}. For any individual in a specific population P_j, the probability of having the genotype G_i at SNP S_i is:

$$p_{ij} = \begin{cases} f_{ij} * f_{ij} & if\ G_i = AA \\ 2 * f_{ij} * (1 - f_{ij}) & if\ G_i = AB \\ (1 - f_{ij}) * (1 - f_{ij}) & if\ G_i = BB \end{cases}$$

The log-transformed likelihood function (L_j) that describes the probability of any individual from population P_j having exactly the same genotypes as the analyzed samples at a specific set of SNPs would be:

$$log_{10}(L_j) = log_{10}\left[\prod_{i=1}^{n} p_{ij}\right] = \sum_{i=1}^{n} log_{10}(p_{ij}).$$

Therefore, the log-transformed likelihood ratio for population P_j compared to the reference population P_0 is:

$$log_{10}(L_j/L_o) = \sum_{i=1}^{n} \left[log_{10}(p_{ij}) - log_{10}(p_{i0}) \right]$$

The likelihood ratio for each population was used to assign ethnicity. “European Ancestry” was assigned to samples for which the two highest-score populations were CEU and TSI. “African Ancestry” was assigned if the four highest-score populations were YRI, ASW, LWK and MKK. “Asian Ancestry” was assigned if the three highest-score populations were JPT, CHD, and GIH. “Hispanic Ancestry” was assigned if the highest-score population was MEX. “Mixed” was assigned as the default ancestry if none of the above conditions could be met.

5. RNA Isolation and Exon Array Processing

5.1. RNA extraction

A bead mill homogenizer (Bullet Blender, Next Advance) was used to lyse the pulverized tissue. Each pulverized tissue sample was transferred to a chilled safe-lock microcentrifuge tube (Eppendorf). A mass of chilled stainless steel beads (Next Advance, cat# SSB14B) equal to the mass of the tissue was added to the tube. Two volumes of Buffer RLT (Qiagen) were added to the tissue and beads. Samples were mixed in the Bullet Blender for 1 min at a speed of six. Samples were visually inspected to confirm desired homogenization and then incubated at 37 °C for five min. Buffer RLT was added up to 0.6 ml, and samples were mixed in the Bullet Blender for 1 min. Total RNA was extracted using a non-phenolic procedure (RNeasy Plus Mini Kit, Qiagen), followed by DNase treatment (TURBO DNase, Ambion) as per manufacturers’ instructions. Optical density values of extracted RNA were measured using a NanoDrop (Thermo Scientific) to confirm an A_{260}:A_{280} ratio above 1.9. RNA integrity number (RIN) was determined for each sample using Bioanalyzer RNA 6000 Nano Kit or Bioanalyzer RNA 6000 Pico Kit (Agilent), depending upon the total amount of RNA.

5.2. Exon array hybridization

Exon array hybridizations were performed at the Yale Center for Genome Analysis and at Gene Logic Inc. (Gaithersburg, MD). Reverse transcription (RT) was performed to generate cDNA from total RNA using RT primers designed using an oligonucleotide matching algorithm. For the selective cDNA synthesis, the Ambion WT Expression kit (Ambion) was used in combination with the GenechipWT Terminal Labeling and Controls Kit (Affymetrix) for target preparation, according to manufacturer recommendations. PolyA controls were added to the input RNA to measure efficiency of target amplification. Fragmented and labelled second cycle cDNA (5.5 µg) was added to a hybridization cocktail prior to loading of 200 µl onto individual Affymetrix Human Exon 1.0 ST arrays. Microarrays were hybridized at 45 °C for 16–24 hours, washed and stained using an Affymetrix FS450 fluidics station, according to manufacturer recommendations. Microarrays were scanned on a GeneChip Scanner 3000 and visually inspected for hybridization artefacts. Exon chip analysis was performed using Affymetrix Power Tools 1.12.0. Probe level data was summarized into probe set level data using the Robust Multichip Average (RMA) background correction algorithm in combination with an R-script. The raw image files (.DAT files) were analyzed using Affymetrix GeneChip Operating Software to generate CEL files.

5.3. Exon array quality assessments

Quality assessment of chip data was performed to reduce errors due to spatial artefacts on the chips, technical differences between chips in probe saturation, differences in the intensity of the probes along the 5’to 3’ gradient of genes, or due to other unaccounted batch effects. First, an idealized reference chip was constructed for all arrays hybridized at each facility by computing the 15% trimmed mean of the log2-transformed probe intensities for each of the 5.5 million perfect match probes across all arrays. Spatial artefacts were defined as severe non-random spatial patterns in the ratios of intensities of probes on one chip relative to corresponding

probes on the ideal reference chip; such artefacts are believed to arise from non-uniform hybridization conditions across the surface of an array. By design, microarray probes are randomly distributed across an array to avoid spatial biases, i.e., probes that represent adjacent regions on the genome are not located physically adjacent on an array. Consequently, in the absence of spatial artefacts due to error sources in pre-processing steps, one would expect a random pattern of probes with higher or lower intensities relative to the reference chip. Supplementary Figure 5 shows ratio intensity plots for arrays with severe spatial artefacts. Chips showing such artefacts were discarded and corresponding RNA reprocessed (N=20). In addition, exon array hybridization uniformity is estimated by gene expression uniformity from 5'-end to 3'-end (Supplementary Fig. 6). To evaluate the possibility of batch effects, four identical samples were submitted to and processed at different testing centers. The correlation was high for these samples processed at two different sites (Spearman correlation r^2=0.967±0.007).

5.4. Exon array pre-processing

Partek Genomics Suite version 6.5 (Partek Incorporated, St. Louis, MO, USA) was used to normalize raw exon array data and to summarize expression of the probe set and transcript cluster. Affymetrix CEL files that passed QC analysis were imported into Partek Genomics Suite using the default Partek settings: RMA background correction[58], quantile normalization, mean probe set summarization, and log2 transformation. Only high-quality core probe sets, as defined by Affymetrix, were included. These high-quality core probe sets have reliable annotations from RefSeq (www.ncbi.nlm.nih.gov) or Ensembl (www.ensembl.org). Data sets were annotated according to the UCSC human genome hg19 reference sequence (http://genome.ucsc.edu/cgi-bin/hgGateway). The median of all individual probe sets of one transcript cluster was used as the estimate of gene expression values. To filter out low expression signals (including noise or poorly hybridized probes), which may lead to false positives, detection above background (DABG) *P*-values for each exon probe sets and transcript clusters were calculated for the probe set and the transcript cluster using Affymetrix power tools (APT, http://www.affymetrix.com/partners_programs/programs/developer/tools/powertools.affx). A mean *P*-value for each probe set or gene was obtained and probe sets or genes with mean *P*-values <0.01 were considered to have expression levels distinct from background level.

5.5. Detection of outliers

We also used correlation analysis to screen potential outliers by comparing an array with others from the same regions and periods. First, Spearman's correlation coefficient tables containing the correlation coefficients for all pairs of arrays from the same region and the same period were generated. The averaged correlation coefficient of each sample was then calculated. We used 3 standard deviations (3 x SDs) as a cut-off to detect outlier. A sample whose averaged correlation coefficient is lower than 3 SDs from the mean value was considered an outlier and was excluded from the study (N=1).

6. Exon Array Data Analysis

6.1. Gene-level analysis

Core probe sets were averaged to yield gene summary values for 17,641 transcript clusters. To consider a gene "expressed" in a particular tissue region/area or at a particular time period, we required it to have a mean DABG *P*<0.01 and log2-transformed expression value >6 in a region/area, irrespective of its temporal regulation.

6.2. Identification of spatial and temporal DEX genes

Analysis of variance (ANOVA) was used to identify differentially expressed (DEX) genes across all regions of interest and during all periods (1-15). Genes that were DEX in at least one brain region or NCX area (spatial DEX) were identified based on ANOVA by using a region/area as a single ANOVA factor. Genes differentially expressed in at least one time period (temporal DEX) were identified based on ANOVA using a

period as a factor. Resulting *P*-values from ANOVA were corrected for multiple comparisons using the Benjamini and Hochberg false discovery rate (FDR) method[59]. A conservative statistical threshold, FDR <0.01 and minimum fold difference >2 between brain regions/areas or periods, was used to identify DEX genes. Genes that were not significantly expressed above background were excluded from ANOVA tests.

To identify among spatially DEX genes that are selectively enriched or restricted in one region (NCX, AMY, HIP, STR, MD, or CBC), irrespective of their temporal regulation, we used a combination of t-test and fold difference analyses. We limited this spatial DEX analysis to periods 3-15, when regions/areas of interest are defined using equivalent criteria and can be consistently followed across time. To consider a gene to be highly or selectively enriched or restricted in one region, a gene has to have more than 2-fold higher averaged signal intensity level during either fetal development (periods 3–7), postnatal development (periods 8–12), or adulthood (periods 13–15). To calculate the fold difference in averaged signal intensity, two regions were used: the region of interest and, from the remaining regions, the one that had the highest averaged expression value. The t-test was then applied to determine if the signal intensity of the gene in one brain region was significantly higher. We employed the Benjamini and Hochberg procedure to generate lists of selectively enriched genes from the t-test *P*-values, and further imposed the criterion that the fold change must be at least two.

6.3. Analysis of gender differences

Genes differentially expressed between males and females were identified by the combination of t-test and fold difference analysis. The two-sample t-test was applied to determine if the expression level of a gene in male samples was significantly different from the expression level in female samples in the same region over periods 3–7, periods 8–12, and periods 13–15. Sixteen brain regions/areas (OFC, DFC, VFC, MFC, M1C, S1C, IPC, A1C, STC, ITC, V1C, AMY, CBC, HIP, STR, MD) were analyzed. The *P*-values from the t-tests were transformed to FDR using the Benjamini and Hochberg method[59]. For each gene, the fold difference (log 2-transformed) between male and female samples in each region over periods 3–7, periods 8–12, and periods 13–15 was also calculated. FDR cutoff of 0.01 and 2 fold difference was used as a cutoff to identify genes that are differentially expressed between males and females.

6.4. Exon-level analysis of alternative exon usage

To identify expressed genes that exhibit differential alternative exon usage (DEU) across all regions of interest and during all periods, we used the combination of the splicing ANOVA method embedded in Partek Genomics Suite and the splicing index (SI) algorithm[60]. In the SI algorithm, normalized intensities were calculated as the expression of an individual exon relative to the expression of the gene, and splicing index was defined as the fold difference of the normalized intensities of exons between two groups (periods and regions). Both spatial DEU and temporal DEU were analyzed. For spatial DEU, the ANOVA factor is set as the brain region/area. All periods were tested and the maximum of splicing indexes among regions was calculated. For temporal DEU, the ANOVA factor is set as the period. Sixteen regions/areas (OFC, DFC, VFC, MFC, M1C, S1C, IPC, A1C, STC, ITC, V1C, AMY, CBC, HIP, STR, MD) were tested, and the maximum of splicing indexes among periods was calculated. Resulting *P*-values from ANOVA were corrected for multiple comparisons using the Benjamini and Hochberg FDR method[59]. To detect meaningful DEU, stringent criteria, *P*-values (FDR < 0.01) and maximum splicing index > 2, were used, and exons expressed at low levels or with low variance (standard deviation of exon expression level <0.5 in all samples, which indicates they are very likely to be saturated in all samples) were excluded.

6.5. Transcriptional profiling of neurobiological processes

The existing lists of genes implicated in neurobiological processes by gene ontology (GO) analysis are highly inclusive, variably sourced, and may not accurately reflect the trajectories of human neurodevelopment. Therefore, we manually curated functional gene lists for specific neurobiological processes and cell types presented in this study: dendrite development (*MAP1A, MAPT, CAMK2A*), excitatory synaptogenesis (*SYP, SYPL1, SYPL2, SYN1*), and cortical GABA cell type markers (*CALB1, CALB2, NOS1, PVALB, VIP*).

To summarize the principle gene expression profile of each category, PCA was performed. The resulting first principal component (PC1) was plotted against logarithmic age in days, and a cubic spline curve was fitted to display the developmental trajectories (Fig. 7). For categories with only one gene, the expression level was used as PC1. To test the accuracy of this strategy, three gene expression trajectories, the *DCX* gene, pan-synaptic genes, and dendrite development genes, were compared with independently generated, non-transcriptome data sets for DCX-positive cell density, synaptic density, and the number of basal dendrites in the corresponding brain regions/areas. PC1 and the independent data were scaled by $\frac{x-\mu}{\sigma}$. μ and σ are the mean and the standard deviation of values, respectively, corresponding to the time periods for which both our gene expression and the independently generated data were available. Our scaled gene expression data were used to generate a cubic spline curve, and the predicted values on this curve were calculated corresponding to available time points of previously generated independent data on DCX[45], dendrite development[46,47], and synaptogenesis[48], which used samples at different time points but within our defined periods. We then calculated the correlation coefficient between our predicted data and the actual values.

6.6. Weighted gene co-expression network analysis

6.6.1. Data set filtering

Only samples from periods 3–15 were included in the weighted gene co-expression network analysis (WGCNA) this analysis. During these periods, brain regions and NCX areas are well defined using equivalent criteria and can be consistently followed across time. NCX areas were not present in periods 1 and 2. Gene co-expression analyses are particularly sensitive to the presence of systematic biases in microarray data. Therefore, we computed pair-wise Pearson correlations of all samples. The inter-array correlations (IACs) were averaged for each array and compared with the resulting distribution. Samples with an average IAC more than 2 SDs below the mean IAC for the data set were excluded from the WGNCA analysis.

6.6.2. Network construction and module detection

To reduce noise, only genes with log2-intensity values greater than 6 in at least one sample and a coefficient of variance greater than 0.08 were used. A total of 8,474 genes fit those criteria. Signed weighted gene co-expression network analysis was performed using WGCNA R package[62]. General information about network analysis methodology and WGCNA software is available at www.genetics.ucla.edu/labs/horvath/CoexpressionNetwork. Pair-wise Pearson correlation coefficients were calculated for all genes selected. The resulting Pearson correlation matrix was transformed into a matrix of connection strengths (an adjacency matrix) using a power function (connection strength = sign (correlation) * |correlation|$^{\beta}$), which was then converted to a topological overlap matrix. WGCNA seeks to identify modules of densely interconnected genes by hierarchical clustering based on topological overlap[63]. The first principal component of each module was calculated and smoothed by cubic spline against log10 (age in days). The top 50 genes expressing the highest within module connectivity were selected and exported to Visant for network visualization. Functional annotation was performed using DAVID Bioinformatics Resources 6.7 (http://david.abcc.ncifcrf.gov/).

6.7. Expression trajectories and gene correlations for autism and schizophrenia-related genes

A list of genes commonly associated with autism was obtained from a recent review by Matthew State[12] (*FMR1*, *NLGN4X*, *NRXN1*, *SHANK2*, *NLGN3*, *CNTN4*, *CNTNAP2*, *SYNGAP1*, *DLGAP2*, *EN2*, and *MET*). A list of genes commonly associated with schizophrenia was obtained from http://www.szgene.org/topresults.asp database; those genes with assigned overall grade A by the database, indicating the highest/strictest association, were included in the analysis (*PRSS16*, *PGBD1*, *NRGN*, *NOTCH4*, *PDE4B*, *TCF4*, *DRD4*, *DAOA*, *TPH1*, *HTR2A*, *MDGA1*, *APOE*, *DISC1*, *AKT1*, *PLXNA2*, and *SRR*).

To generate representations of dynamics in spatiotemporal expression of representative genes (*CNTNAP2, MET, TCF4*, *NRGN*), a heatmap matrix was created for each of these genes according to the

following method. For each combination of developmental period and brain region/area, the log2-transformed expression level values of related samples were averaged to obtain a single value of expression level at the specific period and specific region/area. All of these average values were collected into a data matrix, where each row represents one brain region/area and each column represents one period. After the matrix was created, a heatmap plot was created using R function 'heatmap.2' in package 'gplots'.

The top 50 genes ranked by their correlation with individual genes previously linked related to autism and schizophrenia are presented in Supplementary Table 9 and 10. Genes with the highest correlation to the disease related genes were grouped, respectively, and subjected to functional annotation using DAVID Bioinformatics Resources 6.7 (http://david.abcc.ncifcrf.gov/).

7. Validation Studies

7.1. Quantitative real time RT-PCR and semi-quantitative RT-PCR

An aliquot of the total RNA that was previously extracted from each brain region was used for secondary validation through real-time PCR analysis. One µg of total RNA was used for cDNA synthesis using SuperScript III First-strand synthesis Supermix (Invitrogen) and subsequently diluted with nuclease-free water to 1 ng/µl cDNA. Gene-specific high-melt temperature primers for genes of interest were designed using NCBI/Primer-BLAST (http://www.ncbi.nlm.nih.gov/tools/primer-blast/) and expressed sequence information obtained from GenBank (NCBI). PCR reactions were conducted on an ABI 7900 Sequence Detection System (Applied Biosystems) using a hot start SYBR-green based method (Fast SYBR Green Master Mix, ABI) followed by melt curve analysis to verify specificity of the product. The C_T value (cycle number at threshold) was used to calculate the relative amount of mRNA molecules. The C_T value of each target gene was normalized by subtraction of the C_T value from housekeeping genes to obtain theΔC_T va lue. The relative gene expression level was shown as $2^{-\Delta C_T}$. All genes of interest were normalized to the housekeeping gene *GAPDH*.

Semi-quantitative RT-PCR was performed using the same template and hot start Taq DNA polymerase (Qiagen) under the following conditions: activation at 95 ºC for 10 min, followed by 30–40 cycles at 94 °C for 30 sec, 56 °C for 30 sec, 72 ºC for 60 sec, and extension at 72 ºC for 10 min. The cycling conditions were chosen so that none of the templates analyzed reached a plateau at the end of the thermal cycling, i.e., they were in the exponential phase of amplification. PCR products were separated on a 2% agarose gel and photographed using UV illumination to visualize ethidium bromide labelling. Images were inverted in Adobe Photoshop.

7.2. Immunohistochemistry

Brain tissue samples were fixed in 4% PFA for 2–3 days at 4 °C. Following fixation, tissue was cryoprotected in graded sucrose solutions (up to 30%) at 4 °C, then frozen at -40 °C in 2-methylbutane (J.T. Baker), and stored at -80 °C. Alternatively, fixed tissue samples were paraffin-embedded for routine neuropathological evaluations.

Frozen tissue samples were cut at 60 µm using a Leica CM3050S cryostat and either mounted onto Superfrost/Plus slides (Fisher Scientific Co.) or used free-floating. Tissue sections were incubated in 1% hydrogen peroxide/PBS to quench endogenous peroxidase activity. Sections were washed in PBS (3 x 15 min) and incubated in blocking solution containing 5% (v/v) normal donkey serum (Jackson ImmunoResearch Laboratories), 1% (w/v) bovine serum albumin, and 0.4% (v/v) Triton X-100 in PBS for 1 h at room temperature. Primary antibodies were diluted in blocking solution and incubated with tissues sections overnight at 4 °C. Sections were washed with PBS (3 x 15 min) prior to being incubated with the appropriate biotinylated secondary antibodies (Jackson ImmunoResearch Labs) for 1.5 h at room temperature. All secondary antibodies were raised in donkey and diluted at 1:200 in blocking solution. Sections were subsequently washed in PBS and incubated with avidin-biotin-peroxidase complex (Vectastain ABC Elite kit; Vector Laboratories) for 1 h at room temperature. Finally, sections were washed in PBS (3 x 15 min) and

signal was developed using a DAB peroxidase substrate kit according to the manufacturer's protocol (Vector Laboratories). Following washes in PBS, sections were mounted on Superfrost Plus charged slides, dried, dehydrated, and coverslipped with Permount (Fisher Scientific Co.). Sections were digitized using ScanScope scanner (Aperio). Digitized images were assembled in Adobe Photoshop and Illustrator.

8. Supplementary References

51. O'Rahilly, R. & Müller, F. *The Embryonic Human Brain. An Atlas of Developmental Stages*. (Wiley-Liss, 2006).
52. Poliakov, G.I. (1949) Structural organization of the human cerebral cortex during its ontogenetic development. In: Sarkisov, S.A., Filimonov, I.N. & Preobrazhenskaya, N.S. (Eds.) *Cytoarchitectonics of the Human Cerebral Cortex*. pp. 33-91 (Medgiz, 1949). (in Russian).
53. Sidman, R.L. & Rakic, P. (1973) Neuronal migration, with special reference to developing human brain: A review. *Brain Res* **62**:1-35.
54. Sidman, R.L., & Rakic, P. Development of the human central nervous system. In: Haymaker, W. & Adams, R.D. (Eds) *Histology and Histopathology of the Nervous System.* pp. 3-145 (C.C. Thomas Publisher, 1982).
55. Kostović, I. & Judaš, M. Early development of neuronal circuitry of the human prefrontal cortex. In: Gazzaniga, M.S. (Ed.) *The Cognitive Neurosciences*. pp. 29-47 (MIT Press, 2009).
56. Judaš, M. (2010) Prenatal development of the human fetal telencephalon. In: Prayer D (Ed) Medical Radiology - Diagnostic Imaging. Springer-Verlag. DOI: 10.1007/174_2010_119. (in the press)
57. Brodmann, K. *Vergleichende Lokalisationslehre der Grosshirnrinde in ihren Prinzipien dargestellt auf Grund des Zellenbaues*. (Johann Ambrosius Barth Verlag,1909).
58. Irizarry, R.A., Ooi, S.L., Wu, Z. & Boeke, J.D. Use of mixture models in a microarray-based screening procedure for detecting differentially represented yeast mutants. *Stat Appl Genet Mol Biol.* **2**, Article 1 (2003).
59. Benjamini, Y. & Hochberg Y. Controlling the false discovery rate: a practical and powerful approach to multiple testing. *J R Stat Soc Series B Stat Methodol.* **57**, 289-300 (1995).
60. Okoniewski, M.J. & Miller, C.J. Comprehensive analysis of Affymetrix exon arrays using BioConductor. *PLoS Comput Biol* **4**, e6 1-6 (2008).
61. Cleveland, W. S. Robust locally weighted regression and smoothing scatterplots. *J. Amer. Statist. Assoc*. **74**, 829–836 (1979)
62. Langfelder, P. & Horvath S. WGCNA: an R package for weighted correlation network analysis. *BMC Bioinformatics.* **9**, 559 (2008).
63. Zhang, B. & Horvath, S. A general framework for weighted gene co-expression network analysis. *Stat Appl Genet Mol Biol.***4**, Article 17 (2005).
64. Kostovic, I. et al. Zagreb research collection of human brains for developmental neurobiologists and clinical neuroscientists. *Int. J. Dev. Biol* **35**, 215-230 (1991).
65. Ulfig, N. Calcium-binding proteins in the human developing brain. *Adv Anat Embryol Cell Biol* **165**, III-IX, 1-92 (2002).
66. Meyer, G. Genetic control of neuronal migrations in human cortical development. *Adv Anat Embryol Cell Biol*. **189**, 1-114 (2007)

9. Supplementary Tables

Supplementary Tables are provided in a single Microsoft Excel file.

10. Supplementary Figures

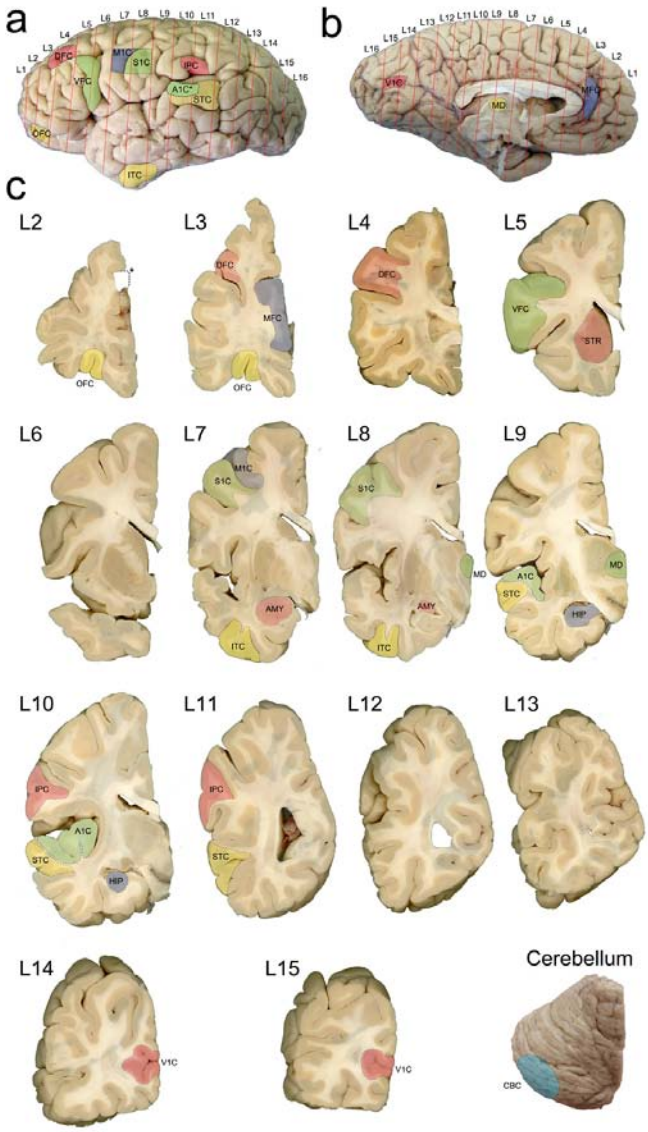

Supplementary Figure 1 | Demarcation of the adult brain regions and NCX areas. a-c, Representative adult human brain images from period 14 are shown illustrating the sampling locations of tissues used for transcriptome analysis. Relative positions of the regions of interest are depicted on lateral (a) and medial (b) surfaces of the hemisphere and dorsal surface of the cerebellar hemisphere (c). Relative sizes of the sampled regions of interest are depicted on coronal slices (c, L2 – L15) of the left cerebral hemisphere. Red lines in (a) and (b) represent cutting lines. The posterior side of the slice is always shown and the average thickness is 1 cm. Brain regions and NCX areas of interest are represented by different colors and two or three letter abbreviations (see Table 2 or section 2.2 of the Supplementary Information). A1C* is located on the temporal bank of the lateral sulcus (i.e. planum temporale and transverse gyrus of Heschl), and cannot be observed on the lateral view of the hemisphere. For illustrative purposes only, relative size and position of the A1C* was depicted on the lateral surface. The dotted line and asterisk (L2) depict an artefact during tissue processing. For detailed sampling procedures see section 2.2 of the accompanying Supplementary Information. These images were generated using fixed brain specimens not used for the exon array analysis.

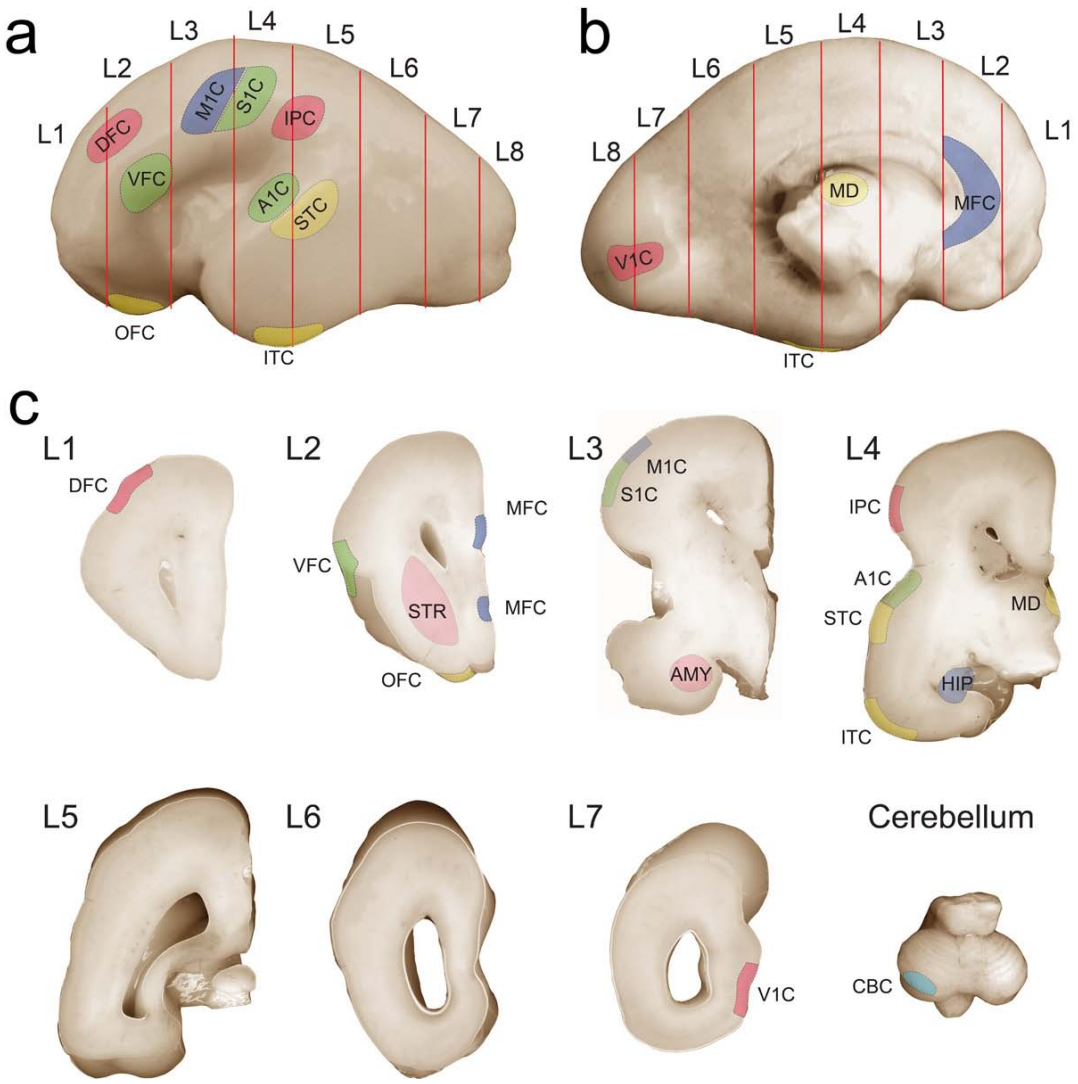

Supplementary Figure 2 | Demarcation of the fetal brain regions and NCX areas. a, b, Representative fetal human brain images from period 6 are shown illustrating the sampling locations of tissues used for transcriptome analysis. Relative positions of the regions of interest are depicted on lateral (a) and medial (b) surfaces of the hemisphere and dorsal surface of the cerebellar hemisphere (c). Relative sizes of the sampled regions of interest are depicted on coronal slices (c, L1 – L7) of the left cerebral hemisphere. Red lines in (a) and (b) represent cutting lines. The posterior side of the slice is always shown and the average thickness is 0.5 cm. Regions of interest are represented by different colors and two or three letter abbreviations (for full names see section 2.2 of the accompanying Supplementary Information). In total, 16 regions of interest were sampled as follows: 5 regions of interest from frontal lobe cortex (OFC, DFC, VFC, MFC and M1C), 2 regions of interest from parietal lobe cortex (S1C and IPC), 4 regions of interest from temporal lobe cortex (A1C, STC, ITC and HIP), 1 region of interest from occipital lobe cortex (V1C), 3 regions of interest from subcortical structures (MD, AMY and STR) and 1 region of interest from cerebellum (CBC). At periods where the M1C and S1C area could not be definitively separated, a single area termed MSC was sampled from the same position as shown here for the M1C and S1C. Sampled regions of interest always contained cortical plate and part of the underlying subplate zone. For detailed sampling procedures see section 2.2 of the Supplementary Information. These images were generated using fixed brain specimens not used for the exon array analysis.

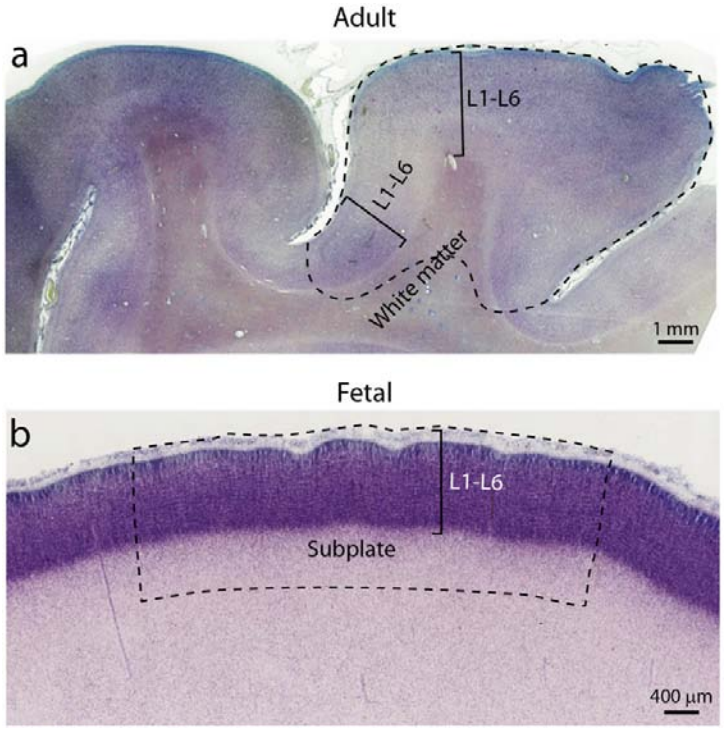

Supplementary Figure 3 | Demarcation of adult and fetal NCX areas at the microscopic level. a, b, Nissl staining images of the adult (a, period 14) and fetal (b, period 6) VFC are shown to illustrate the microscopic boundaries of the NCX tissue sampled for transcriptome analysis. In the adult brains (a) all six cortical layers (L1 – L6) and underlying gyral white matter were sampled. In the fetal brains (b) entire cortical plate (L1 – L6) and adjacent subplate zone was sampled. Dotted lines in (a) and (b) represent dissection boundaries. These two images were generated using fixed brain specimens not used for the exon array analysis.

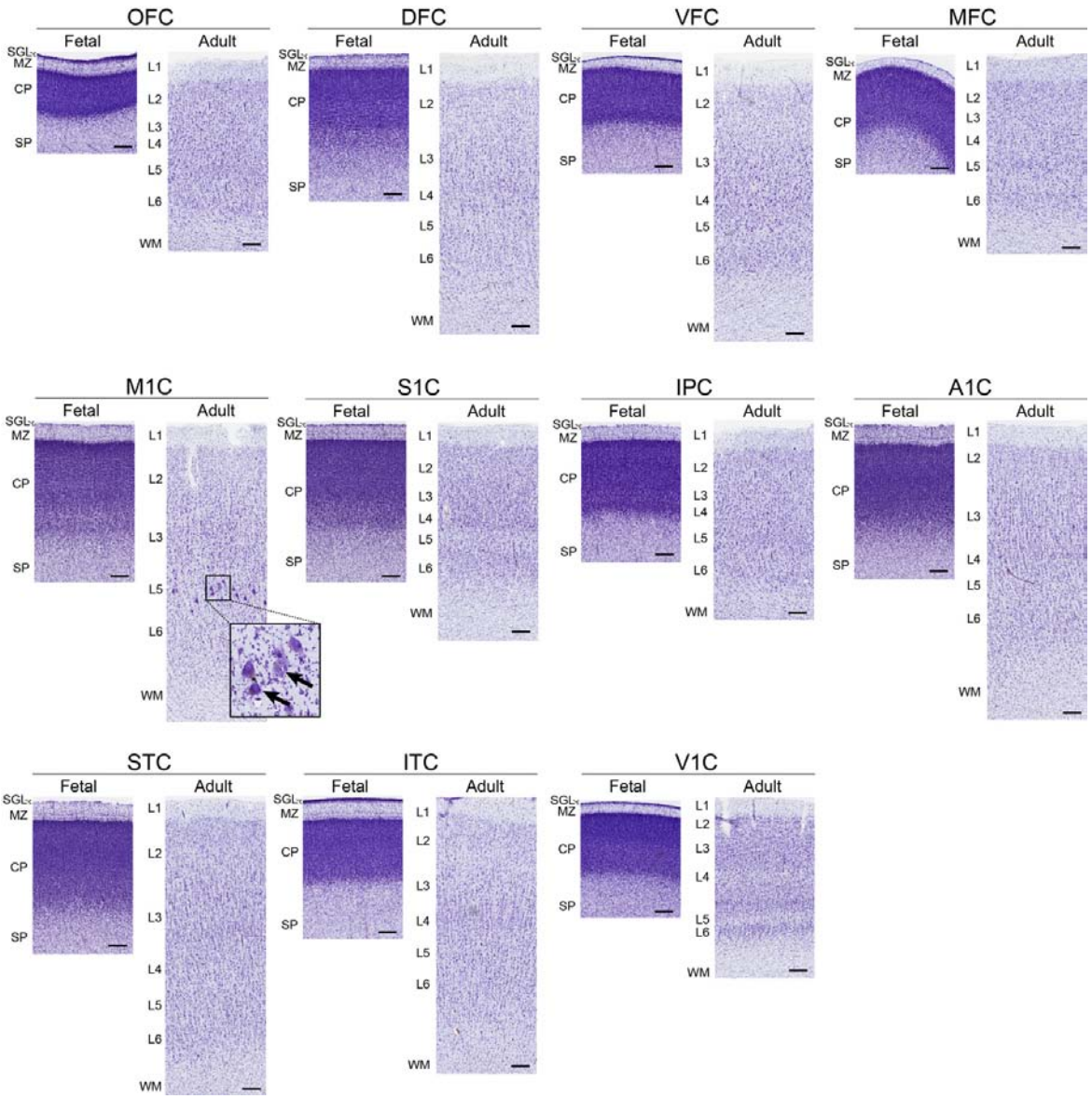

Supplementary Figure 4 | Validation and comparison of fetal and adult NCX areal cytoarchitecture. Nissl staining was used to validate the following NCX areas: OFC, DFC, VFC, MFC, M1C, S1C, IPC, A1C, STC, ITC, and V1C. Sampling from fetal (period 6) and adult (period 14) specimens was carried out according to the methods and criteria used for the dissection of exon array samples. Staining in fetal NCZ areas revealed densely packed neurons in the cortical plate (CP) with no obvious distinctions among cortical layers. The subpial granular layer (SGL), marginal zone (MZ), and subplate (SP) were present in the fetal samples. Conversely, adult NCX neurons were at a lower density and were arranged in layers (L1-L6) containing neurons of distinct size and shape (e.g., L5-specific Betz cells in M1C; arrow). The adult cortical layers had a greater thickness than the fetal cortical plate, and white matter (WM) was apparent below the laminar pattern. Scale bars, 250 μm.

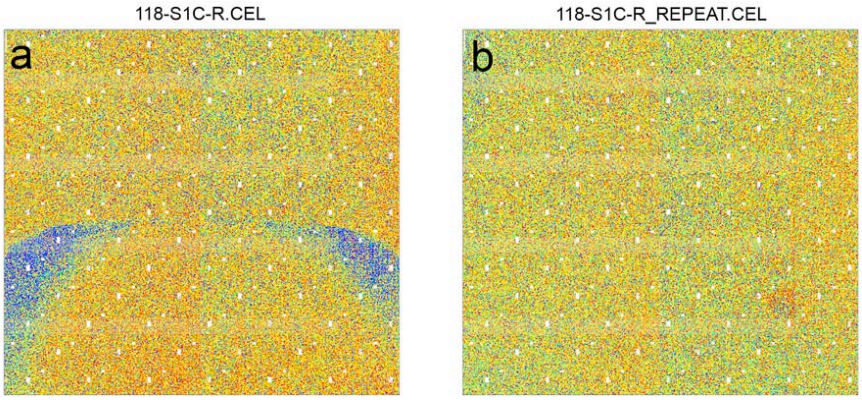

Supplementary Figure 5 | Representative images of intensity plot of exon array for low and high quality. The color of each dot in the plot represents relative intensity of a probe in the target chip compared to the average intensity of that probe in the same batch of chips. Individual probes of one gene were randomly located on the whole chip, and consequently there should be no obvious spatial pattern in the plot. **a**, Relative intensity plot of a low quality chip for sample 118-S1C-R with spatial artefacts. **b**, Relative intensity plot of the high quality replicate chip for the same sample (118-S1C-R_REPEAT), without obvious spatial artefact.

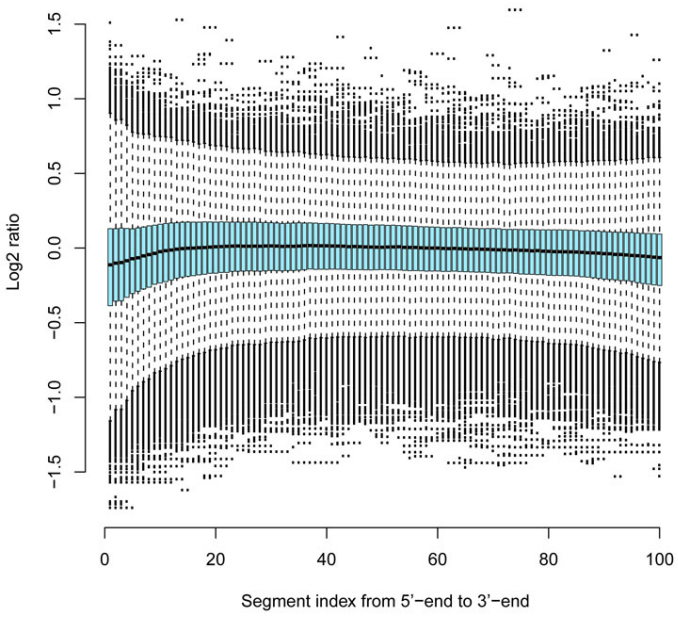

Supplementary Figure 6 | Illustration of exon array hybridization uniformity. The longest transcription of each gene was split into 100 segments with equal length, from 5'-end to 3'-end, and the log2-transformed signal intensity ratio for each segment was calculated compared with the expression of the whole gene across 1,316 chips. The statistics of the ratios for all genes were displayed by a box plot for each segment. The flat solid line consisting of the mean lines of box plots displays the array hybridization uniformity.

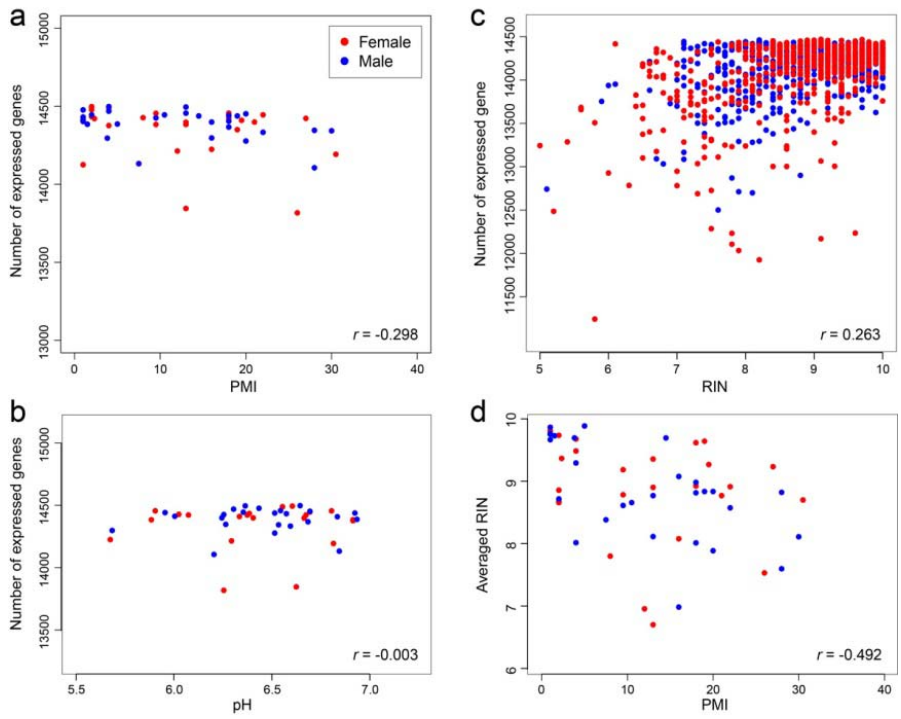

Supplementary Figure 7 | Correlations between PMI, pH, RIN, and gene expression. a,b, Correlation of number of expressed genes with PMI (a) and pH (b). Each data point represents one brain. Week anticorrelation was observed with PMI (Spearman correlation, r = -0.298) and no correlation was observed with pH (Spearman correlation, r = -0.003). **c**, Correlation between number of expressed gene with RIN. Each data point represents one sample. A weak correlation was observed (Spearman correlation, r = 0.263). **d**, Correlation between PMI and RIN. Each data point represent one brain specimen, Y-axis is the averaged RIN of individual brain specimens. X-axis is PMI of the same specimens. The Spearman correlation is -0.492, indicating that PMI and RIN are anticorrelated.

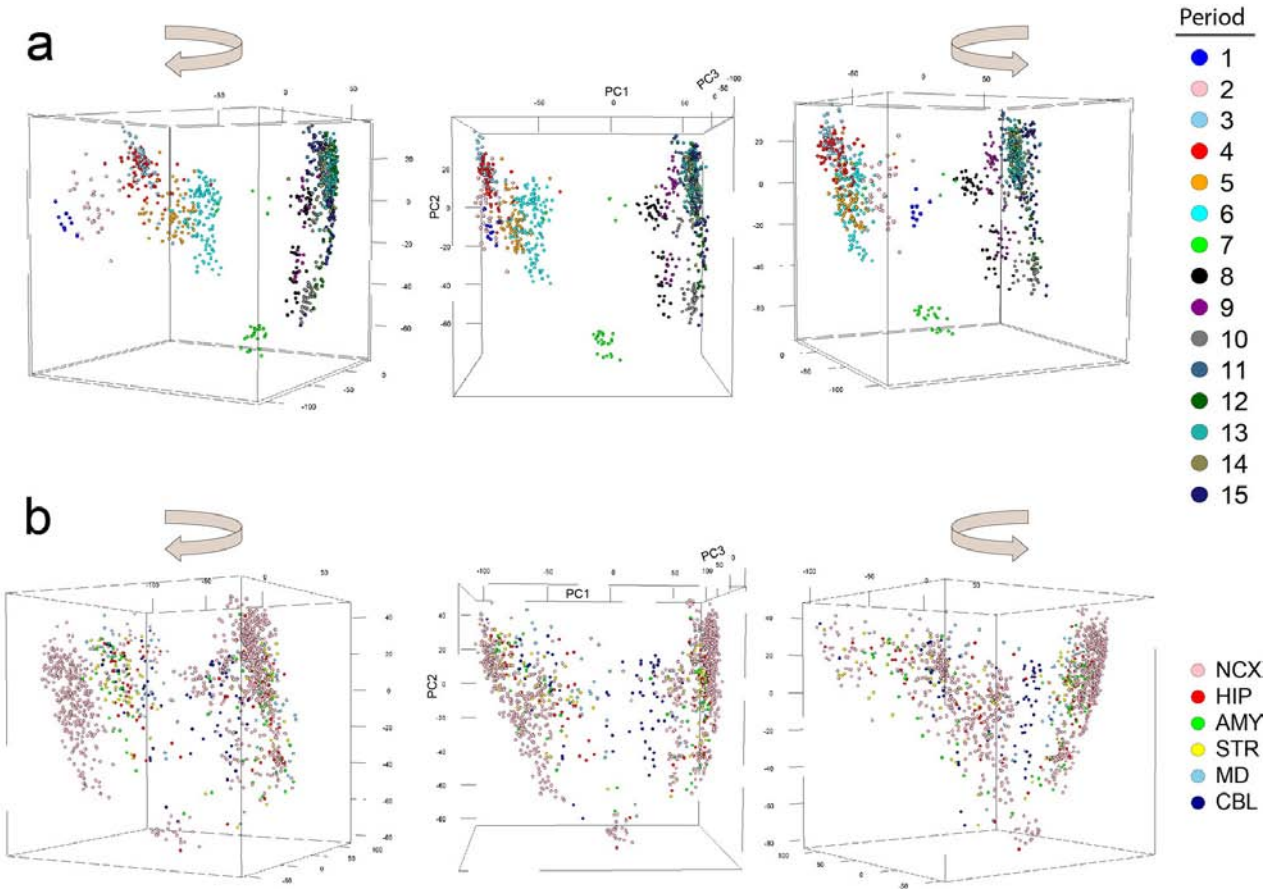

Supplementary Figure 8 | Principal component analysis (PCA). a, Three-dimensional plot of PCA of NCX samples across 15 time periods. Each point represents one NCX sample. Samples are colored by period. Three dimensional figures are rotated to make a better view of the separation within prenatal (extremely left) and postnatal (extremely right) periods. **b**, PCA plot for all 1,316 samples across 6 brain regions and all time periods. Each point represents one sample. Samples are colored by brain region.

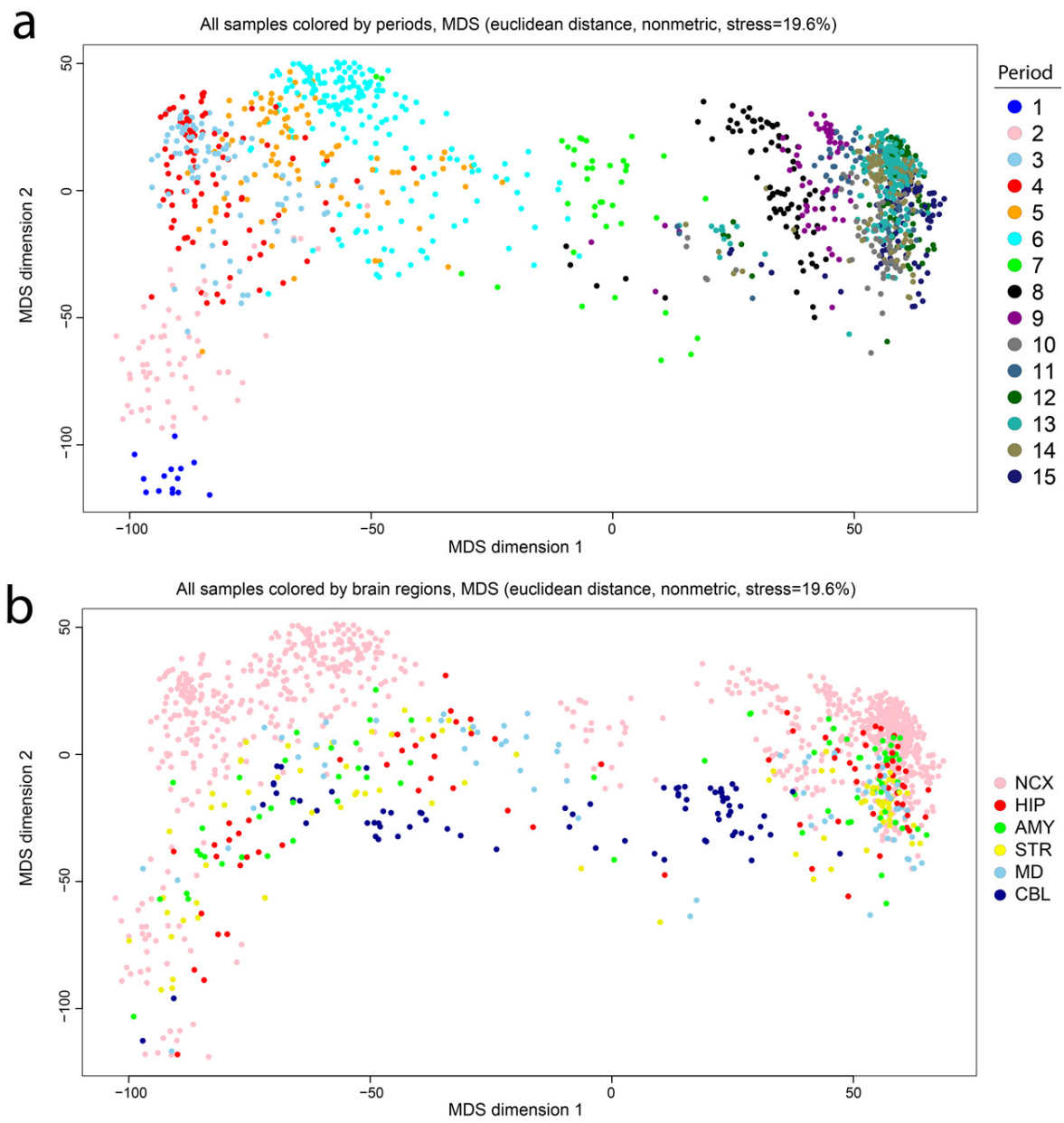

Supplementary Figure 9 | Multi-dimensional scaling (MDS). a, b, Two-dimensional MDS plot showing genome-wide transcriptional dissimilarity between any two samples throughout 15 time periods (a) and regions (b). Each sample was represented as a single point. Proximity indicates transcriptional similarity between two samples, while distance indicates dissimilarity. Euclidean distance of log2-transformed signal intensity (expression) values were used to measure the pairwise dissimilarity. The isoCMD function in the R package was used to create the configuration of all points in the two dimensional space. Samples were colored by time period (a) or region (b).

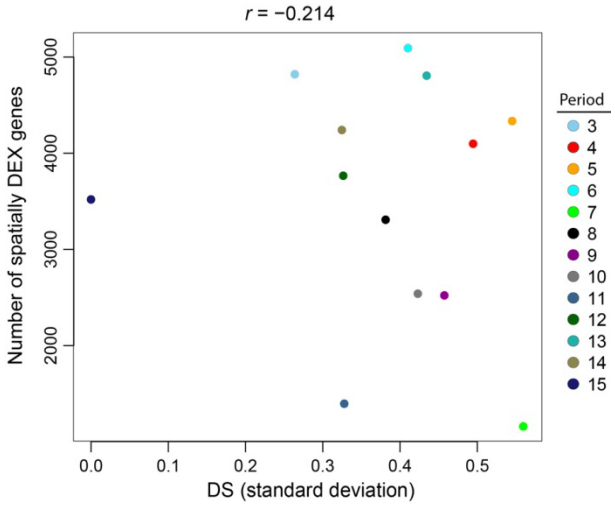

Supplementary Figure 10 | Correlations between the dissection score (DS) and DEX genes. The Y-axis is the number of spatially DEX genes with significantly differential expression between brain regions and NCX areas detected by ANOVA test (FDR <0.01 and 2-fold difference) for the particular period. The X-axis is the standard deviation (SD) of DS of all samples in that period. No significant correlation was observed between variation of dissection score (DS) and number of spatially DEX genes (Spearman correlation, r = -0.214). We limited this analysis to periods 3-15, when regions/areas of interest are well defined using equivalent criteria and can be consistently followed across time, thus allowing us to assess the impact of variations in DS within the same stage contribute to differences in the number of detected spatially DEX genes for that particular period.

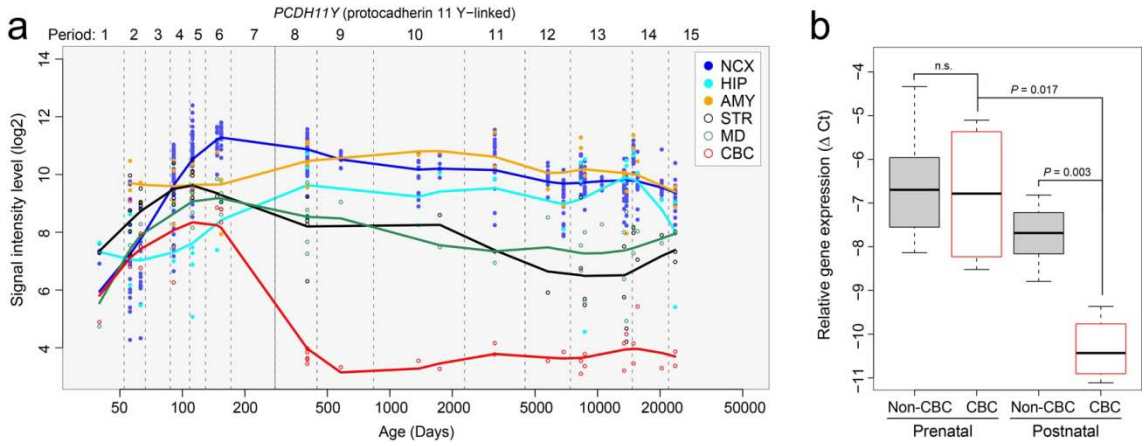

Supplementary Figure 11 | Spatiotemporal differences in *PCDH11Y* expression in males. **a**, Line plots showing the log2-transformed exon array signal intensity values. The solid line separates prenatal from postnatal periods. **b**, Box plot showing the relative expression levels of qRT-PCR (ΔCt,) in non-CBC regions (gray boxplots; NCX, HIP, AMY, STR, MD) and CBC (white boxplots with red outlines) from prenatal or postnatal male specimens. ΔCt value is calculated by subtracting average Ct value of *PCDH11Y* from the Ct value of reference gene, *GAPDH*. n.s., non significant (two-tailed unpaired t-test).

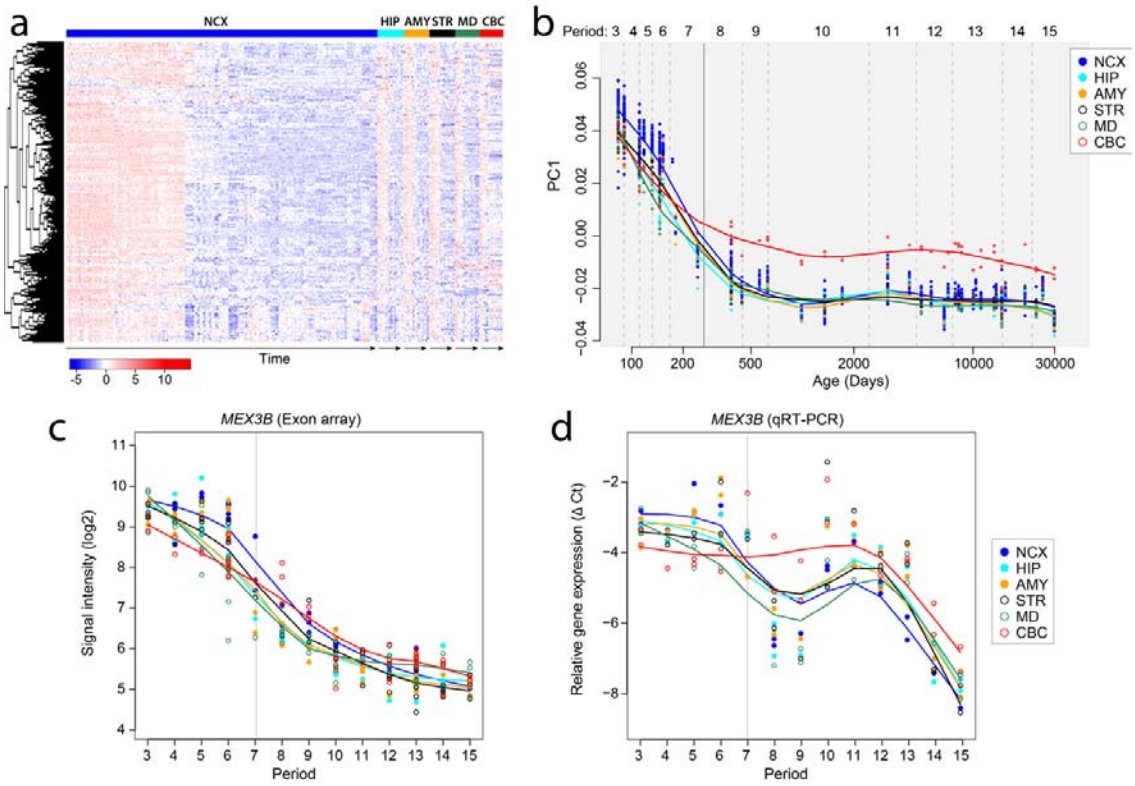

Supplementary Figure 12 | M20 network module. The WGNCA module M20 associated with a progressive decrease in gene expression across all regions starting from the embryonic period. **a**, Heat map of genes in module M20 after hierarchical clustering showing the temporally co-expressed pattern is consistent across all regions. The expression values for each gene are ordered first by brain regions, then by age, and last by NCX areas. **b**, The spatiotemporal pattern of M20 was summarized using PCA analysis. The first component (PC1) was displayed along age, after being grouped and color-coded according to brain regions. The pattern was summarized by the smoothed curves of PC1 values. Dashed lines represent division between periods of the development and the solid line separates prenatal from postnatal periods. **c, d**, Analysis of spatiotemporal expression of a representative gene, *MEX3B*, with high intramodular connectivity revealed a similar pattern to the one observed for the entire M20 module. Line plots show the log2-transformed exon array expression value (c) and relative expression level of quantitative RT-PCR (ΔCt, d) during periods 3-15.

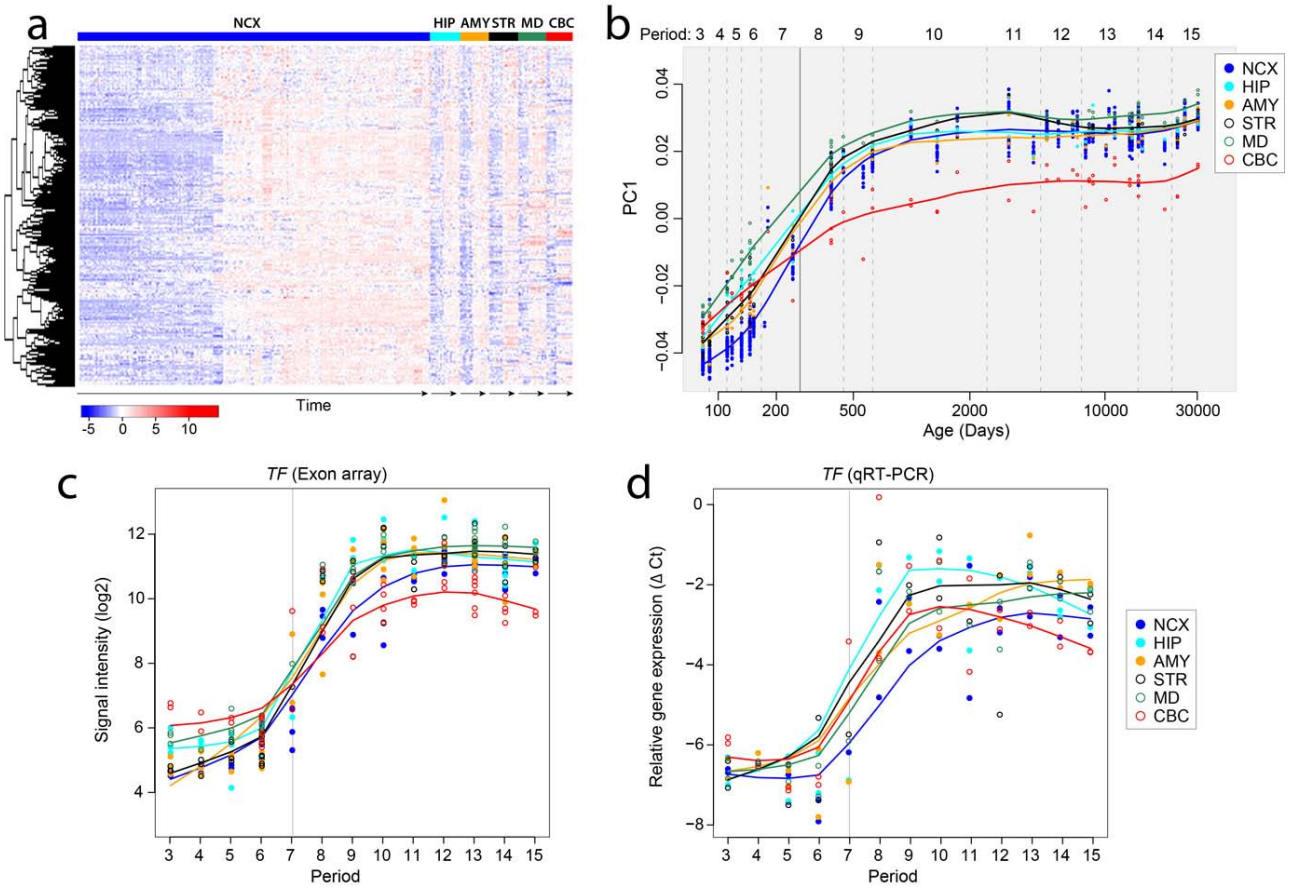

Supplementary Figure 13 | M2 network module. The WGNCA module M2 associated with a progressive increase in gene expression across all regions starting at the embryonic period. **a**, Heat map of genes in module M2 after hierarchical clustering showing the temporally co-expressed pattern is consistent across all regions. The expression values for each gene are ordered first by brain regions, then by age, and last by NCX areas. **b**, The spatiotemporal pattern of module M2 was summarized using PCA analysis. PC1 was displayed along age, after being grouped and color-coded according to brain regions. The pattern was summarized by the smoothed curves of PC1 values. Dashed lines represent division between periods of the development and the solid line separates prenatal from postnatal periods. **c, d**, Analysis of spatiotemporal expression of a representative gene, *TF*, with high intramodular connectivity revealed a similar pattern to the one observed for the entire M20 module. Line plots show the log2-transformed exon array expression value (c) and relative expression level of quantitative RT-PCR (ΔCt, d) during periods 3-15.

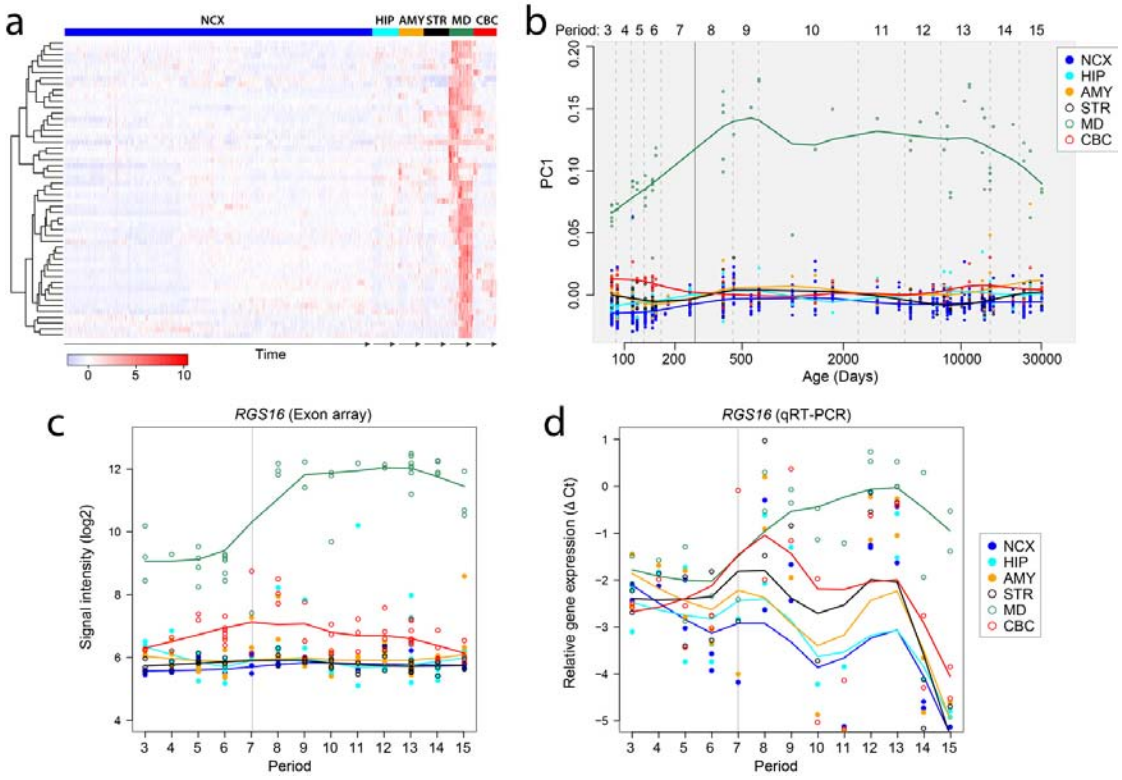

Supplementary Figure 14 | M9 network module. The WGNCA module M9 associated with a specific enrichment in the MD. **a**, Heat map of genes in module M9 after hierarchical clustering showing the spatiotemporal pattern of the module. The expression values for each gene are ordered first by brain regions, then by age, and last by NCX areas. **b**, The spatiotemporal pattern of M9 was summarized using PCA analysis. The first component (PC1) was displayed along age, after being grouped and color-coded according to brain regions. The pattern was summarized by the smoothed curves of PC1 values. Dashed lines represent division between periods of the development and the solid line separates prenatal from postnatal periods. **c, d,** Analysis of spatiotemporal expression of a representative gene, *RGS16*, with high intramodular connectivity revealed a similar pattern to the one observed for the entire M20 module. Line plots show the log2-transformed exon array expression value (c) and relative expression level of quantitative RT-PCR (ΔCt, d) during periods 3-15.

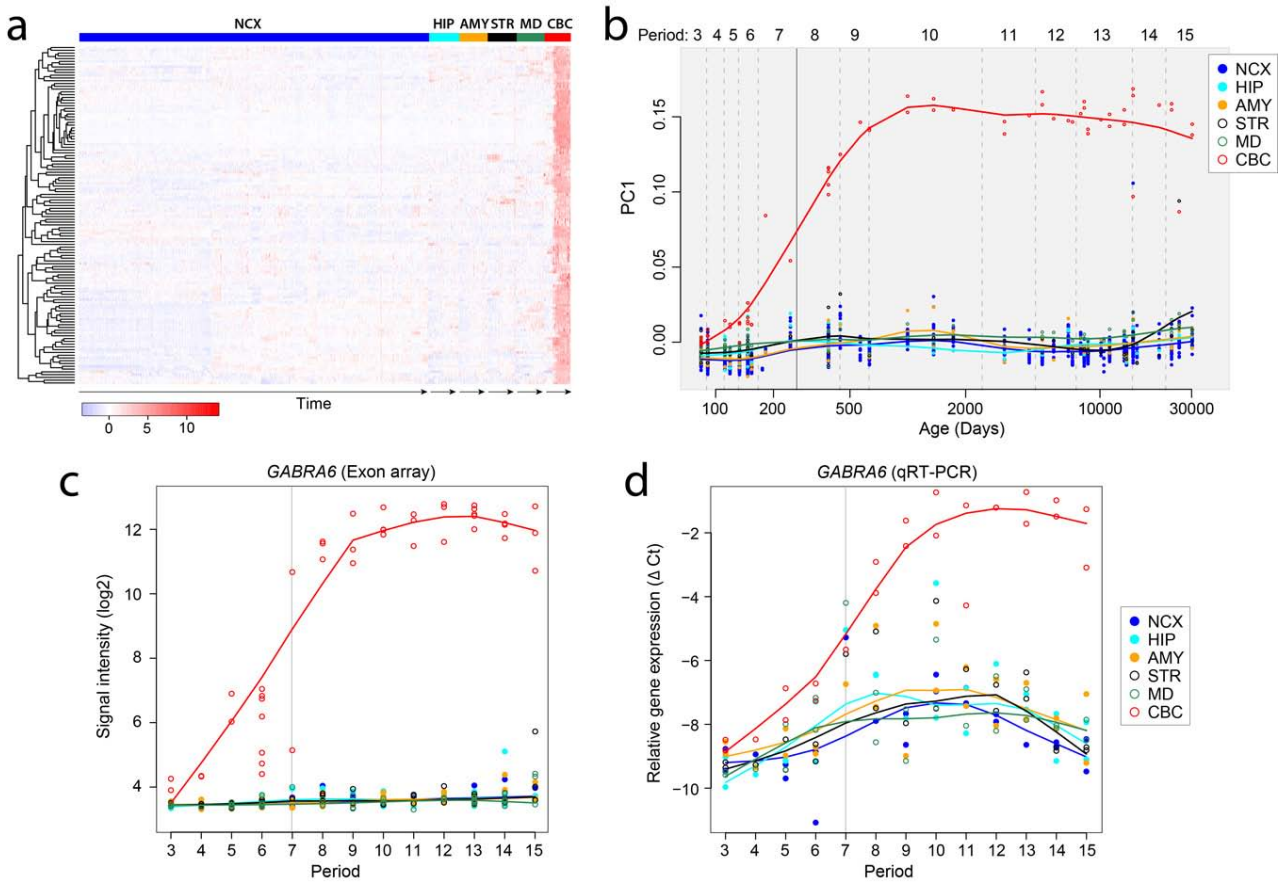

Supplementary Figure 15 | M19 network module. The WGNCA module M19 associated with a specific enrichment in the CBC. **a**, Heat map of genes in module M19 after hierarchical clustering showing the spatiotemporal pattern of the module. The expression values for each gene are ordered first by brain regions, then by age, and last by NCX areas. **b**, The spatiotemporal pattern of M19 was summarized using PCA analysis. The first component (PC1) was displayed along age, after being grouped and color-coded according to brain regions. The pattern was summarized by the smoothed curves of PC1 values. Dashed lines represent division between periods of the development and the solid line separates prenatal from postnatal periods. **c, d**, Analysis of spatiotemporal expression of a representative gene, *GABRA6*, with high intramodular connectivity revealed a similar pattern to the one observed for the entire M20 module. Line plots show the log2-transformed exon array expression value (c) and relative expression level of quantitative RT-PCR (ΔCt, d) during periods 3-15.

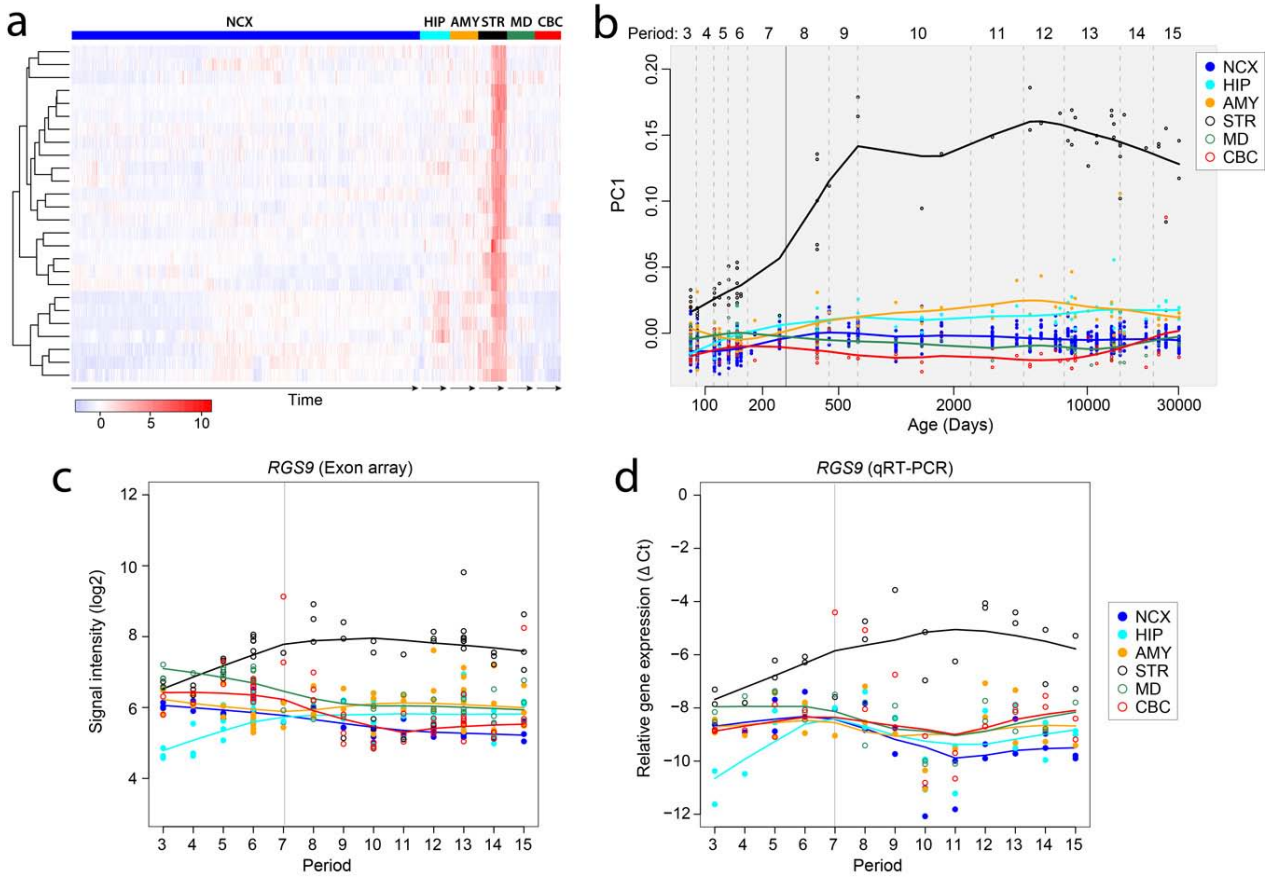

Supplementary Figure 16 | M23 network module. The WGNCA module M23 associated with a specific enrichment in the STR. **a**, Heat map of genes in module M23 after hierarchical clustering showing the spatiotemporal pattern of the module. The expression values for each gene are ordered first by brain regions, then by age, and last by NCX areas. **b**, The spatiotemporal pattern of M23 was summarized using PCA analysis. The first component (PC1) was displayed along age, after being grouped and color-coded according to brain regions. The pattern was summarized by the smoothed curves of PC1 values. Dashed lines represent division between periods of the development and the solid line separates prenatal from postnatal periods. **c, d**, Analysis of spatiotemporal expression of a representative gene, *RGS9*, with high intramodular connectivity revealed a similar pattern to the one observed for the entire M20 module. Line plots show the log2-transformed exon array expression value (c) and relative expression level of quantitative RT-PCR (ΔCt, d) during periods 3-15.

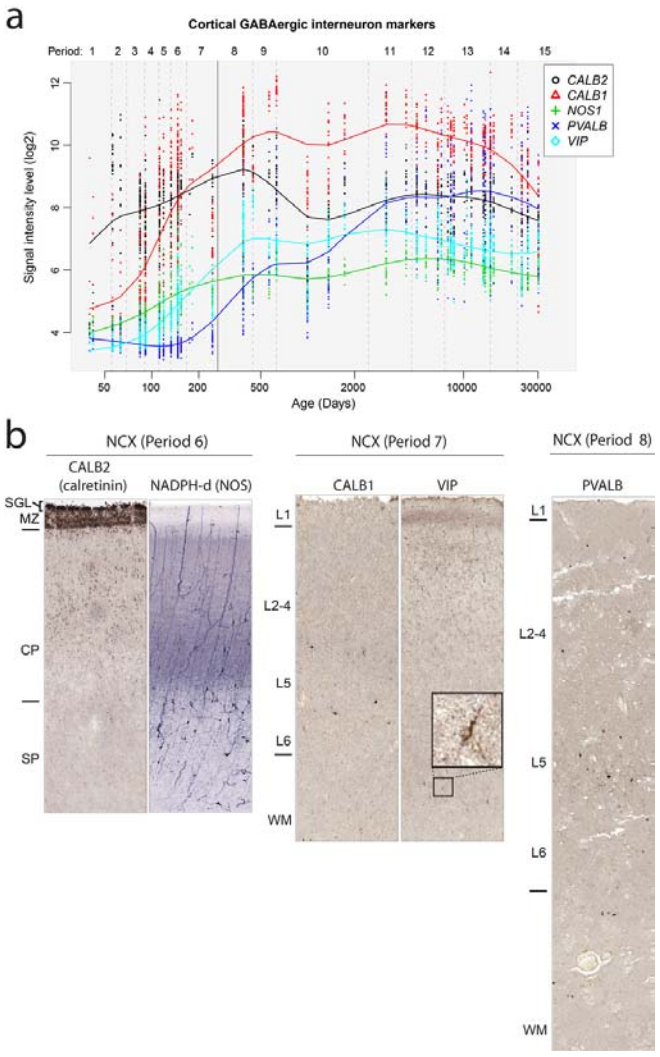

Supplementary Figure 17 | Developmental trajectories of cortical GABAergic interneuron markers. a, Transcriptome-based expression trajectories for commonly used markers of different subclasses of cortical GABAergic inhibitory neurons. **b**, Representative images of immunohistochemical detection of CALB2 (calretinin), NADPH-d (a histochemical marker of NOS, including NOS1), CALB1 (calbindin), VIP (vasoactive intestinal peptide), and PVALB (parvalbumin) in the NCX during periods 6 to 8. Expression trajectories are reminiscent of the changes in the immunohistochemical detection of interneuronal markers in the fetal and early postnatal human NCX. Of the cortical GABAergic interneuron markers analyzed in this study, *CALB2* gene expression is higher than the other markers during periods 1 and 2 (black line in a). Consistently, CALB2-immunopositive interneurons are the most abundant of the analyzed marker of GABAergic interneuron cell types in the NCX during midfetal periods (**b**; see also Ref. 49). Notably, CALB2-immunopositive cells are numerous in the upper part of the cortical plate (CP). Conversely, NADPH-d/NOS1-positive interneurons are less abundant than CALB2-immunopositive interneurons (green line in a). Although some NOS1-positive cells can be found in deeper layers of the CP, the majority is found in the CP-subplate (SP) border. Consistent with the gene expression data and previously independent immunohistochemical studies[64, 65], CALB1- and VIP-immunopositive interneurons are next to be detected in the NCX and can be well identified during period 7. Of the cortical GABAergic interneuron markers analyzed in this study, *PVALB* gene expression (dark blue line in a) and immunohistochemical staining (b) are the last to be detected in the NCX around birth.